

CBPF - CENTRO BRASILEIRO DE PESQUISAS FÍSICAS

Rio de Janeiro

Monografia

CBPF-MO-002/89

NUCLEAR FRAGMENTATION

by

K.C. CHUNG



I. INTRODUCTION

In this decade, the advent of powerful accelerators and the development of new detection techniques have given rise to many interesting experimental data, especially in what concerns to the high-energy heavy-ion collisions.

In fact, in proton-induced heavy-ion collisions at relativistic energies or in heavy-ion induced collisions both at intermediate and high energy regions, the available data show that, as in consequence of the collision, the initial system breaks-up in many pieces. The analysis of the distribution of the remnant fragments, especially those of small-to-medium size, suggests that this process can not be explained by already existing reaction mechanisms such as, e.g., evaporation or fission. It seems, therefore, that we are in front of a new phenomenon, to which one uses to refer as nuclear fragmentation (nuclear multifragmentation also is sometime used). The understanding of this apparently novel process is one of the main goals of the investigations in the field of heavy-ion collisions at intermediate-to-relativistic energies.

On the other hand, it is inescapable to concede that our present understanding of the nuclear matter equation of state $\epsilon = \epsilon(n, T)$ is extremely poor. As a matter of fact, the

unique point in the diagram $T \times n$, experimentally measured, is $n = n_0$, $T = 0$, where n_0 is the normal nucleus number density (around 0.15 fm^{-3}). The behaviour of the nuclear matter in the neighborhood of n_0 plays a crucial role in many fields, e.g., supernova and neutron star calculations, ultra-relativistic heavy-ion collisions, etc. As nuclear fragmentation is a process which results from a system at high density and high temperature, it is expected that it provides useful informations about the nuclear matter equation of state.

The renewed interest in nuclear fragmentation processes is due to, undoubtedly, the Purdue-Fermilab collaboration (Minich et al., 1982) which, in the beginning of this decade, reported results from p+Xe and p+Kr head-on collisions at 80-350 GeV of incident energy. In particular, they plotted the mass yield of light-to-medium size fragments and noted that the mass distribution is best fitted by a power-law than by an exponential. This behaviour, as they have appointed out, is similar to one displayed by the cluster distribution, such as found in the Fisher's condensation model for a molecular Van der Waals system and in the percolation theory for infinite systems (see references below).

This similarity prompted the Purdue group to interpret the nuclear fragmentation results as a signature of a liquid-gas phase transition of the nuclear system at its critical temperature. Although all of us are yet very familiar with changes of state, the interpretation of the nuclear fragmentation as a critical phenomenon provoked an extraordinary interest in this area, both from the experimental and the theoretical

points-of-view. In these last few years, much more experimental data have been worked out and paralelly many theoretical models have been proposed in order to reproduce the main features of the experimental results.

In this course, it is my wish to give an introduction to nuclear fragmentation, with emphasis in percolation ideas. The choice of topics and the reference list reflect only my own point-of-view. I apologize for references and topics which are left out. The course is sketched as the following:

In Sect. II, general concepts are introduced and the relevant experimental results are presented in Sect. III. Sect. IV discuss the main theoretical models, except the percolation models. As an application, we present in Sect. V the uniform expansion approximation and use the statistical multifragmentation model to calculate the fragment energy spectra. Sect. VI is dedicated to percolation models. Finally, summary and conclusions are given in Sect. VII.

II. GENERAL CONCEPTS

Let me recall that experiments on high energy heavy-ion collisions suggest that the results are rather insensitive to the combination of projectile and target nuclei, and that the relevant quantity in this energy range is the total incident energy per particle, instead of the total incident energy. Also, an important quantity to be considered is the impact parameter b . Two extreme cases are of interest, i.e. , $b = 0$ (head-on, collisions) and $b = R_p + R_T$ (peripheral collisions), where R_p and R_T

are the radius of the projectile and the target nucleus, respectively.

In quite general bases, what do we expect to find when two heavy-ions collide at the energy range we are interested in ? In other words, what happens when a projectile nucleus incides on a target nucleus, with a bombarding energy E_{inc}/n ? The picture may be the following: The projectile and the target nuclei merge to form a composite system. This system, after compressed and heated-up, expands and cools down until the system becomes unstable against the formation of heavy fragments (the fragment size A_f is typically less than $1/3 A_T$).

In the collision process, the total incident energy is partly used to remove nucleons from the target (prompt nucleons), or is directly converted into mesonic degrees of freedom. The remaining energy may be stored as compressional energy or transformed into excitation energy of the system.

Unfortunately, there is no straightforward way to relate E_{inc}/n with E^*/n or with the number of fast particles ejected out. Possible approaches would be the intranuclear cascade techniques or hydrodynamical codes.

We can understand in terms of the total excitation energy per particle E^*/n why the system splits in many clusters as soon as the threshold is reached. If E^*/n is sufficiently small, the system undergoes collective oscillations or forms a compound nucleus, but it dissolves completely into free nucleons, if E^*/n is greater than the nucleon binding energy, which is around 8 MeV. Between these two limiting cases, the system becomes unstable against formation of complex fragments

(nuclear fragmentation), which seems to happen at $E^*/n = 3-4\text{MeV}$.

We can also discuss the collisions in terms of the bombarding energy E_{inc}/n . In this case, the Coulomb barrier V_{Coul} (some MeV's in the case of heavy-ions) is the relevant quantity. For low bombarding energies, i.e., $E_{\text{inc}}/n < V_{\text{Coul}}$, we have the complete fusion and for $E_{\text{inc}}/n \gtrsim V_{\text{Coul}}$, the incomplete fusion. Finally, if $E_{\text{inc}}/n > 25\text{ MeV}$, nuclear fragmentation may occur. In the case of proton-induced reactions, the fragmentation threshold is much higher (around 1 GeV) due to the smaller compression the proton provokes in the target nucleus.

The heavy-ion collisions we are interested in may be regarded as a two-step process, i.e.:

- 1) Partition of the total incident energy into the several degrees of freedom of the composite system (collisional stage);
- 2) The unstable system gives rise to the production of heavy fragments (disassembly stage).

The first stage involves a very complex rearrangement of the available energy, but it is with the second stage that the most part of fragmentation models are concerned. Therefore, in this course, we will restrict ourselves to the static models which requires no treatment of the collisional stage at all.

One basic question in nuclear fragmentation is: Could be the nuclear disassembling regarded as a multi-step process in which each step is considered a binary process, such as we find, e.g., in the so-called sequential evaporation? So far, it seems that the answer is no, and in fact a non-conventional explanation is underlying the most part of the theoretical models: a one-step process involving multi-particles (nuclear multifrag-

mentation). The difference in these two approaches is concerned mainly with the timescale of the fragmentation process. In the last point-of-view, this timescale is assumed very short in comparison with the duration of the collisional stage, so that the approximation of a simultaneous break-up (explosive process) can be made. On the contrary, in the first point-of-view, the approximation of very short timescale is not assumed, and the nuclear fragmentation is described as a non-simultaneous process.

As mentioned in the Introduction, nuclear fragmentation is a phenomenon observed in intermediate and high energy collisions. Let's put this in a more precise manner. The intermediate energy domain usually is taken as beginning from the threshold of the cluster formation (~ 25 MeV) and extending to the onset of the high-energy or relativistic regime, ~ 400 MeV/n, corresponding to the energy for which the relativistic parameter $x = p/m_0c = 1$. As much as the intermediate energy regime is concerned, the theoretical approach is expected to be particularly difficult. The reason is that, in this energy regime, it is not possible to resort to approximations neither of the low energy heavy-ion collisions (long mean free path, one-body dissipation, mean field), neither of the high energy case (short mean free path, two-body dissipation).

III - EXPERIMENTAL DATA

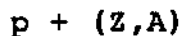
The experimental data concerning nuclear fragmentation are mostly of inclusive character. This means that in the experiment only some of the observables are measured. As an

example, a typical inclusive data is the mass yield, where the fragments are counted irrespectively of its impact parameter. Of course, inclusive data imply loss of information. Exclusive data are related to experiments in which the observables are measured simultaneously. Unfortunately, these kinds of experiment are very hard to perform and in consequence the exclusive data are scarce.

Generally, the inclusive data are presented as the quadrupole differential cross section, $d\sigma^4/dA_f dZ_f dEd\Omega$. When integrated over all charges, energies and angles, we have $\frac{d\sigma}{dA_f}$ which is the cross section for production of fragments with mass number A_f .

The experimental data come from:

a) proton-induced reactions at high-energy,



b) heavy-ion-induced reactions at intermediate and high-energy



and the main observed quantities are:

a) Mass yields

b) Isotopic yields

c) Energy spectra

Let's first present the results from the above-mentioned Purdue-Fermilab experiment (Finn et al., 1982), which concerns with the p+Kr and p+Xe reactions at bombarding energy in the range 80-350GeV. In Fig. 1, it is shown the mass yield of the fragments with $A_f < 30$, for both reactions. The fitting of the experimental points by a power law, i.e.,

$$\text{Yield}(A_f) \propto A_f^{-\tau} \quad (1)$$

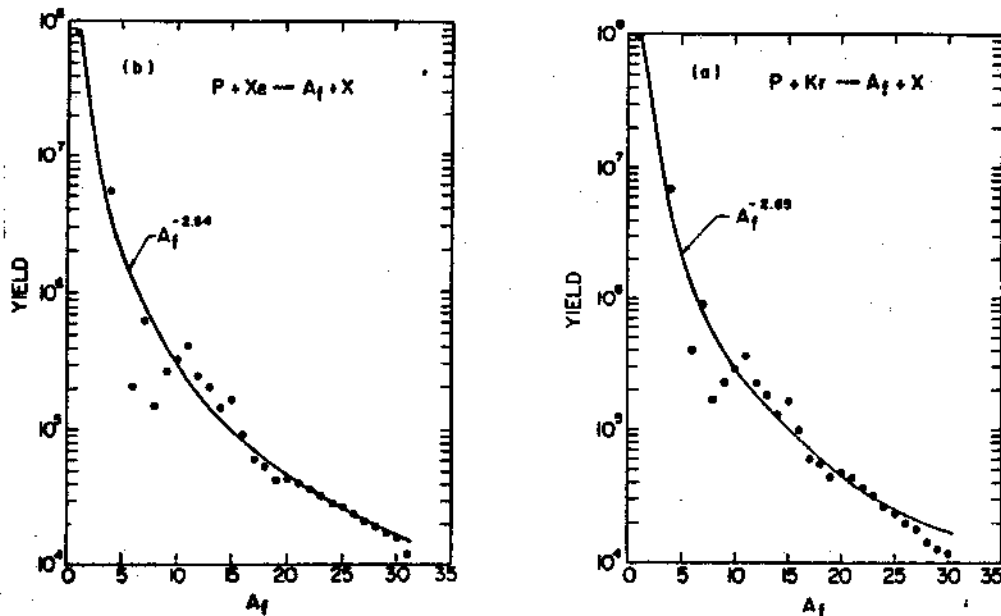


FIG. 1 - Taken from Finn et al. (1982).

gives $\tau = 2.64$ for p+Xe, and $\tau = 2.65$ for p+Kr.

Furthermore, the mass yield is observed not vary significantly for different target nucleus and different incident energy within the above-mentioned range.

Recently, the same group reported (Mahi et al., 1988) that the same experimental data, after reanalysed with a somewhat different procedure, may give an exponent as low as 2.3.

The same behaviour of the mass distribution can be seen also in heavy-ion-induced reactions. Fig. 2 displays the results from the reaction $^{16}\text{O} + ^{197}\text{Au}$ (Berthier et al., 1987), for 60 GeV/n and 200 GeV/n. In the first case, the power law with $\tau = 2.64$ fits very well the data, although in the second case the exponential fits better. Figs. 3 and 4 show the mass yield data from Panagiotou et al. (1985) and from Gutbrod et al. (1982) respectively. Again, the data seems to display a power-law behaviour.

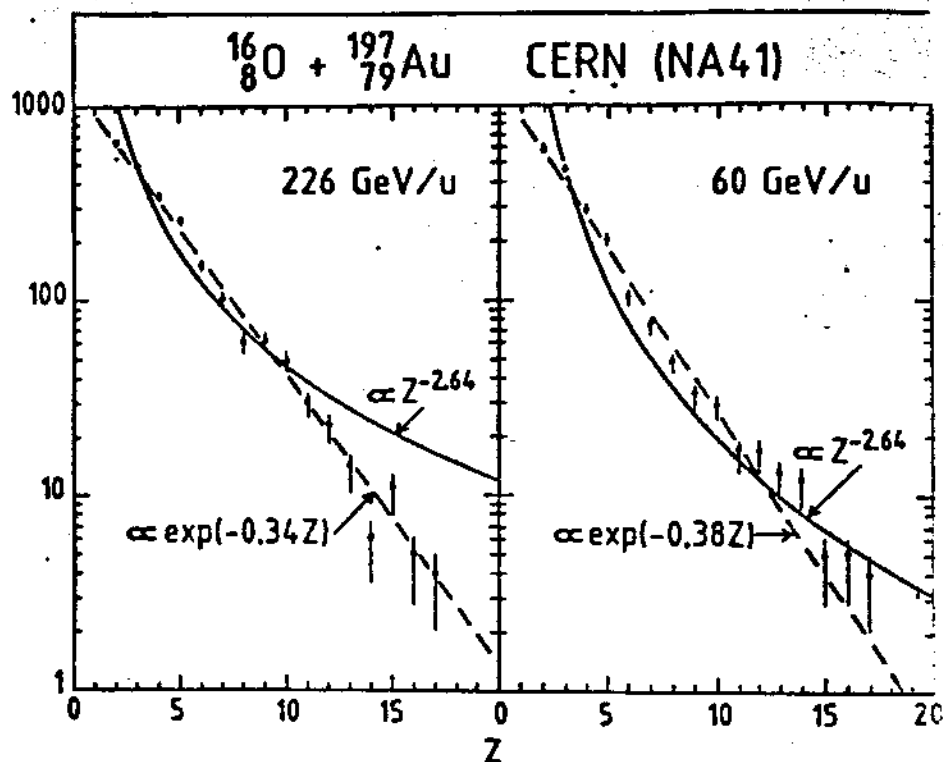


FIG. 2 - Taken from Berthier et al. (1987).

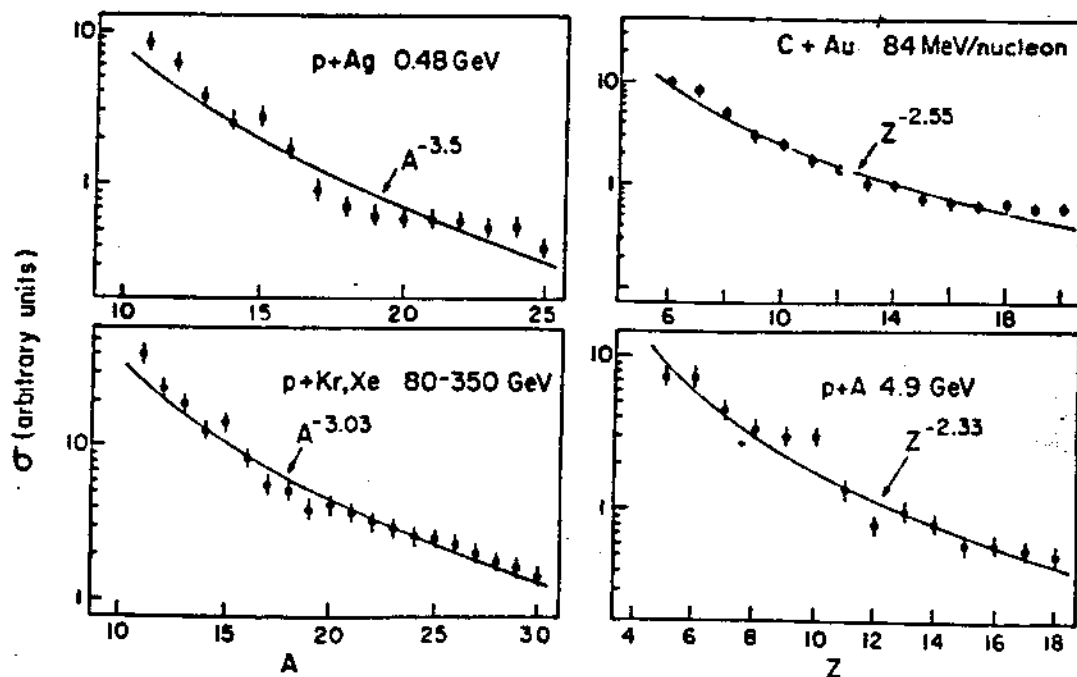


FIG. 3 - Taken from Panagiotou et al. (1985).

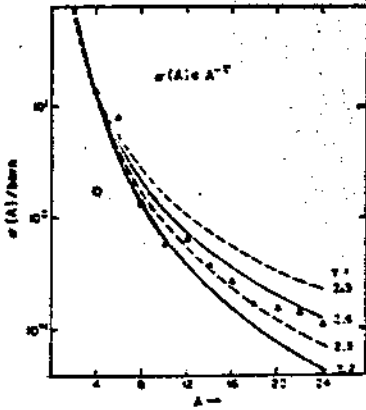


FIG. 4 - Taken from Gutbrod (1982).

The dependence of τ on the incident energy for p+Xe reactions at 1-19 GeV of bombarding energy (Fig. 5) as well as the excitation curves (Fig. 6) were reported by Mahi et al. (1988). It is seen that τ stabilizes around 2.1 for higher incident energies, and that the excitation curves increases very steeply until incident energy around 10 MeV, after that maintains almost constant.

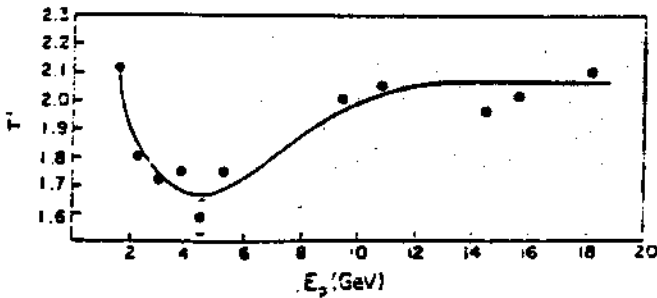


FIG. 5 - Taken from Mahi et al. (1988).

With relation to isotopic yields, Fig. 7 gives the results obtained by Hirsch et al. (1984). The dashed and solid lines are drawn to guide the eye. In (a)-(c), the results refer to p+Kr and in (d)-(f), p+Xe collisions.

Finally, the kinetic energy spectra of ^{12}C and isotopes and of ^{16}O

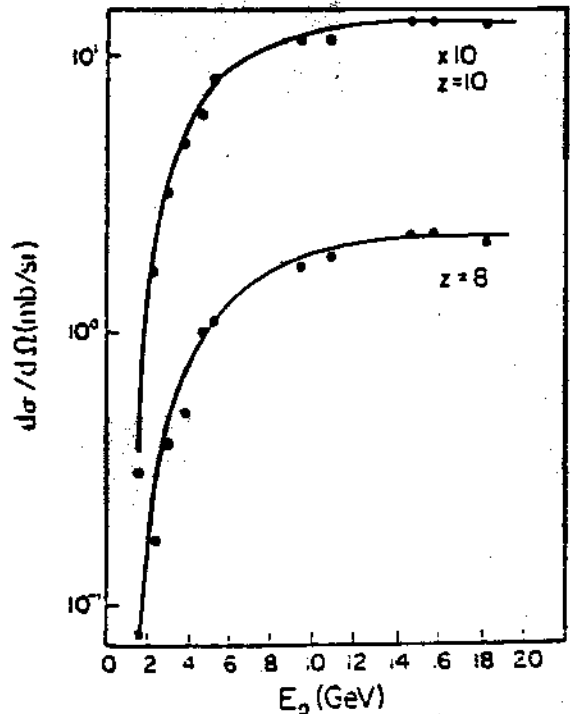


FIG. 6 - Taken from Mahi et al. (1988).

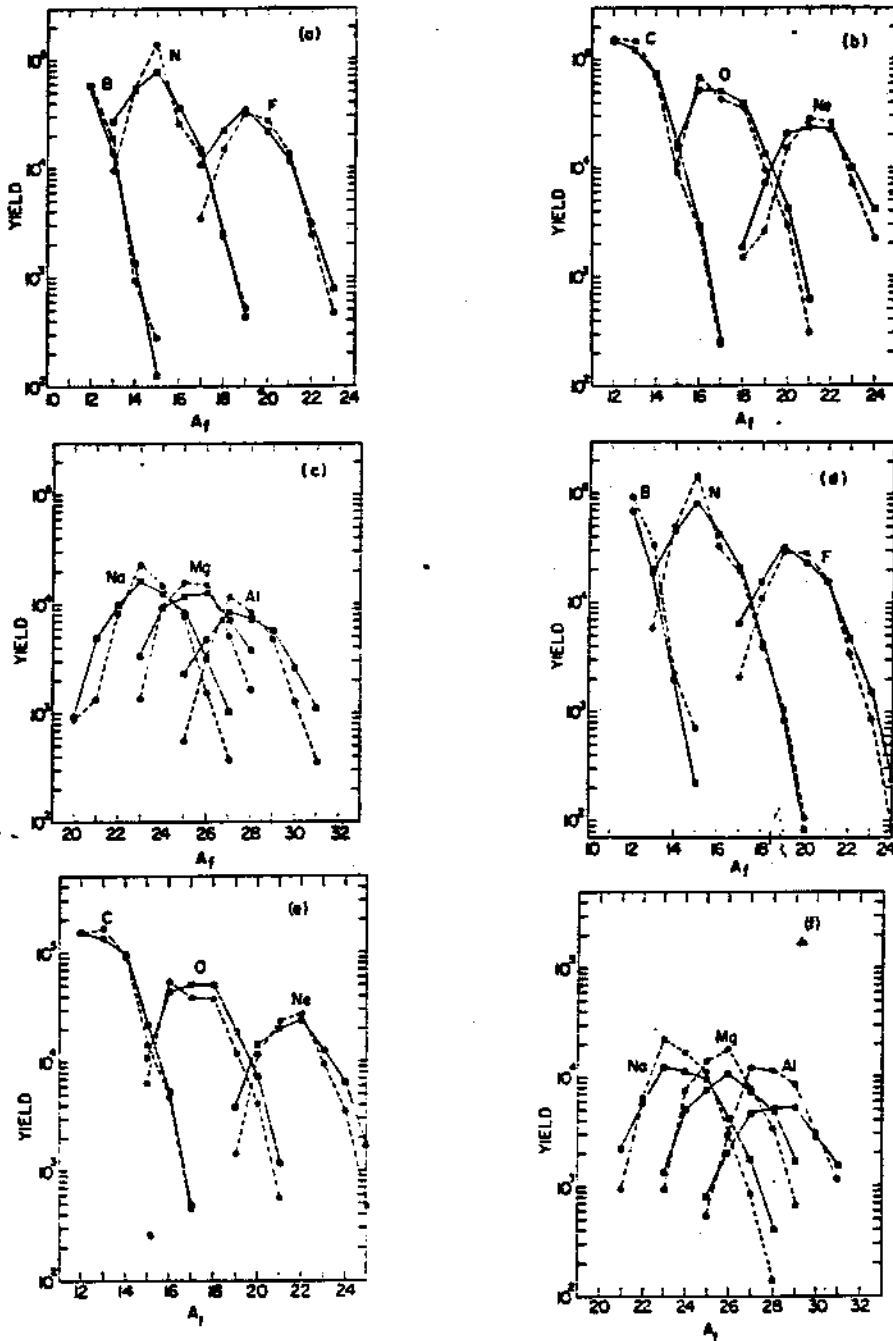


FIG. 7 - Taken from Hirsch et al. (1984).

and isotopes (Fig. 8), taken from Hirsch et al. (1984), are presented. All the curves refer to the p+Kr reaction at bombarding energy of 80-350 GeV and present almost the same shape, with an rapid increasing, followed by a maximum value (around 18MeV for C and isotopes, and 22 MeV for O and isotopes) and finally, an exponential decay. Fig. 9 shows energy spectra from Warwick

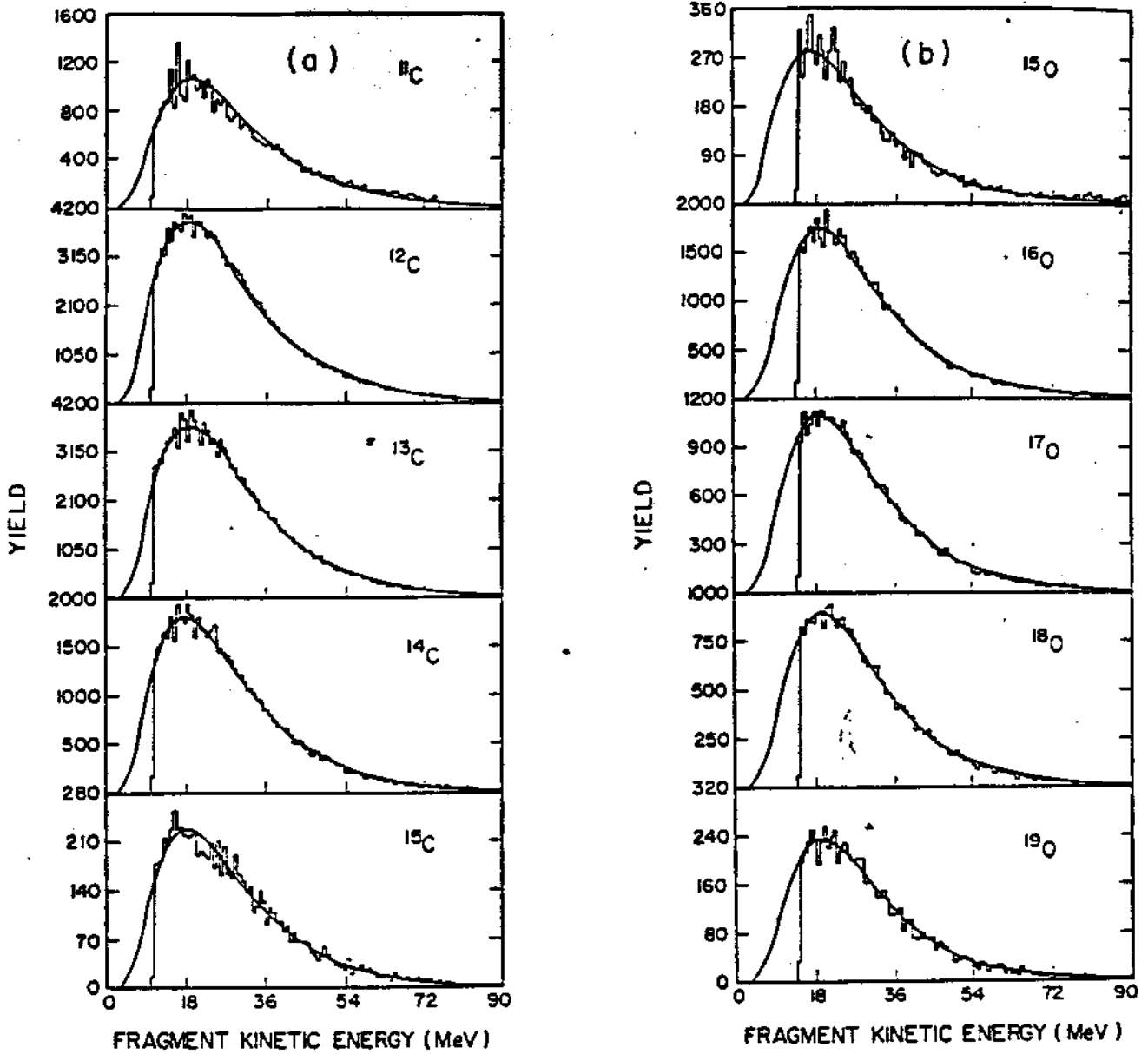
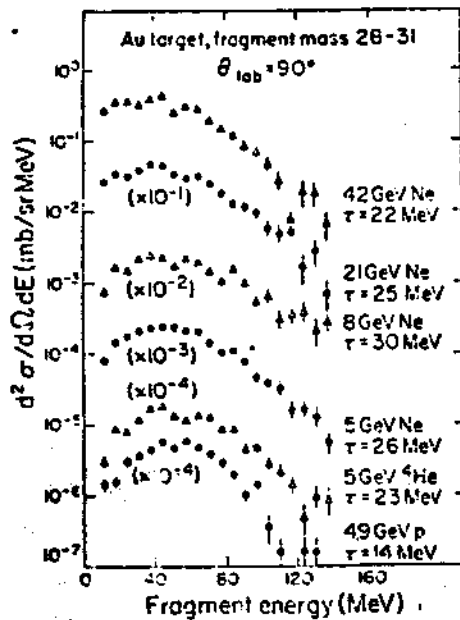


FIG. 8 - Taken from Hirsch et al. (1984).

FIG. 9 - Taken from Warwick (1982).



et al. (1982), with similar behaviour.

IV. THEORETICAL MODELS

Nuclear fragmentation seems to be a very complex phenomenon. Its reaction mechanism is not well understood yet. In what follows, we will restrict ourselves to the discussion of the disassembly stage only, leaving out the collisional stage. This means we will not be concerned with how the colliding system evolves in time until it breaks-up in many pieces (in this respect, see Ngô et al., 1987; Aichelin et al., 1988; Vicentini et al., 1985). We simply assume a hot portion of nuclear matter, which in general is in non-equilibrium state. Therefore, the models we will discuss consider solely the final stage of the break-up.

Basically, some models regard the break-up as the result of thermal instabilities (e.g., statistical multifragmentation model), mechanical instabilities (e.g., cold fragmentation), liquid-gas phase transition, or purely geometrical aspects (percolation approach). Beside this, others assume an usual evaporation/fission mechanism (e.g., sequential evaporation) or simple phase space considerations (statistical models).

So many models, based on so different hypothesis, is likely to reflect a situation of almost complete ignorance.

In the following, we will discuss the most important models of nuclear fragmentation, leaving however the percolation models for the next Section. Let us consider first the most spectacular model, the liquid-gas phase transition model proposed by the Purdue group. In this point, it seems to worthwhile to

review the Fisher's droplet condensation model, on which the liquid-gas phase transition approach is based.

4.1 - Liquid-Gas Phase Transition Model

Basically, Fisher's droplet model (Fisher, 1967) is a generalization of the gas condensation model, first proposed independently by Frenkel, Band and Bijl, a half century ago.

More specifically, they have considered a gas with constituents interacting through short range repulsive forces (hard core) and short range attractive forces. These constituents may consist of isolated molecules or clusters of two or more molecules, which are assumed to be in statistical equilibrium. Experimentally, at low densities and temperatures, this system may undergo an abrupt change from a gaseous to a liquid state (condensation).

The condensation model assumes:

- a) the interactions between clusters can be neglected;
- b) the cluster binding energy $U(A)$ and the cluster entropy $S(A)$, where A is the cluster size, may be splitted into two contributions, i.e.,

$$U(A) = U_0 A + U_1 s \quad (2)$$

$$S(A) = S_0 A + S_1 s \quad (3)$$

where each expression above contains a bulk term (the first one) and a surface term (second one), and s is the surface area of the cluster, U_0 (U_1) and S_0 (S_1) are the binding energy per particle (per area unit) and the entropy per particle (per area

unit), respectively.

It should be noted that the clusters are considered approximately spherical and that $A \rightarrow \infty$. Under these conditions, the probability for the formation of a droplet of size A at temperature T is given by:

$$P(A) \propto A^{-\tau} X^{A^{2/3}} Y^A \quad (4)$$

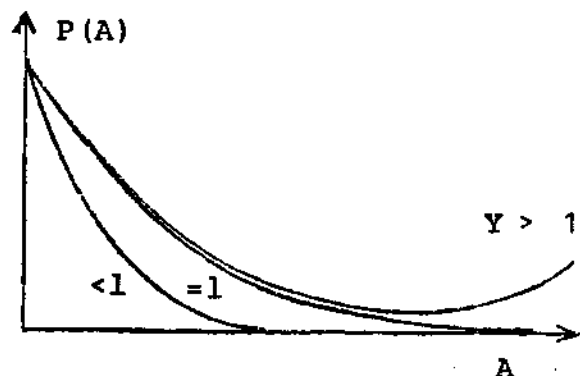
where:

$$X = \exp[-(U_1 - T S_1)/kT]$$

$$Y = \exp[-[(U_0 - T S_0) - \mu]/kT]$$

and μ and τ are, respectively, the chemical potential and the critical exponent. It should be noted that Eq. (4) has much to do with the scaling function in the percolation theory, as it will be discussed in Sect. VI.

In Fig. 10, taken from Fisher (1967), it is plotted $P(A)$ against A , for 3 different values of Y . It is seen that



the larger value of $P(A)$ for very large clusters indicates that the condensation has taken place. So, $Y = 1$ is identified as corresponding to the condensation point.

Furthermore, assuming

FIG. 10 - Taken from Fisher (1967).

that, at $T = T_c$, the surface coefficient vanishes, i.e.,

$$U_1 - T S_1 = 0 \quad , \quad (5)$$

then only the power-law factor survives,

$$P(A) \propto A^{-\tau} \quad (6)$$

It will be shown, in connection with percolation ideas, that the critical exponent τ is in the range

$$2 < \tau < 3 \quad (7)$$

For temperatures away from the critical point, the potential factor is modulated by an exponential. In fact, Eq. (4) is rewritten as

$$P(A) \propto A^{-\tau} \exp[-(F_A - \mu A)\beta] \quad (8)$$

where

$$F_A = U(A) - T S(A) \quad (9)$$

is the Helmholtz free energy and $\beta \equiv 1/kT$.

In order to apply the Fisher's original single-component model to the nuclear case, the Purdue group (Minich et al., 1982) extended it to the two-component case, i.e., to a system with neutrons and protons.

Firstly, $\mu\beta A$ has to be replaced by

$$(\mu_N N_f + \mu_Z Z_f)\beta + (N_f \ln \frac{N_f}{A_f} + Z_f \ln \frac{Z_f}{A_f})$$

where the last term is due to the entropy of neutron and proton mixing, and the subscripts N, Z and f denote, respectively, neutron, proton and fragment.

The Helmholtz free energy is assumed, just as before, having bulk and surface contributions, given by

$$F_A = a_V(T) A + a_S(T) A^{2/3} \quad (10)$$

It is noted that a_V and a_S are functions of the temperature T and each one includes both binding energy and entropy of the cluster. Having in mind that $F_A = E_A - TS_A$, they assume that the entropy has the same functional dependence on the variables than the binding energy. So, they argue that the free energy may have the same analytic form than the binding energy.

Using the parametrization of the Bethe-Weizsacker semi-empirical formula, then

$$F(A_f, Z_f) = a_V A_f - a_S A_f^{2/3} - a_C \frac{Z_f^2}{A_f^{1/3}} - a_{\text{sym}} \frac{(A_f - 2Z_f)^2}{A_f} - \delta \quad (11)$$

where a_V , a_S , a_C and a_{sym} represent, respectively, the volume, surface, Coulomb and symmetry contributions to the free energy, and

$$\begin{aligned} \delta &= a_P A_f^{-3/4} && \text{(odd-odd nuclei)} \\ \delta &= 0 && \text{(odd-even)} \\ \delta &= -a_P A_f^{-3/4} && \text{(even-even)} \end{aligned} \quad (12)$$

Eq. (11) justifies why this approximation is referred as Thermal Liquid-Drop Model.

Using the ideas and equations expressed above, the behaviour of the experimental isotopic yields can be understood. As a matter of fact, from the Fisher's formula, Eq. (4), the charge yield follows:

$$Y(A_f, Z_f) = C A_f^{-\tau} \exp\{[-F(A_f, Z_f) + \mu_N N_f + \mu_Z Z_f] \beta + N_f \ln \frac{N_f}{A_f} + Z_f \ln \frac{Z_f}{A_f}\} \quad (13)$$

where C is a normalization constant.

Then, it is expected that near the critical point, the isotopic yield would be damped with relation to the yield calculated at T. In particular, if we calculate the argument of the exponential, say, for the case of ^{18}N , we find a factor of $\sim 1/100$. The experimental data from Hirsch et al., 1984, (Fig. 7), seems to confirm this behavior. In these data, we can see a large decrease in the yield with relation to the most populated isotope.

By fitting the isotopic yield data, they have found a critical temperature for finite nuclei $T_c \approx 3$ MeV.

This value is far different from the predicted for infinite nuclear matter (≈ 16 MeV, see Ravenhall et al., 1983), and even the one for finite nuclear systems, which was calculated as $\sim 11-12$ MeV via finite temperature Hartree-Fock calculations with Skyrme effective interaction (Jaqaman, Mekjian and Zamick, 1984).

The Purdue group claims that the isotopic yields are completely compatible with the TLDM. They used this to support their interpretation that the power-law behaviour of the isobaric distribution is a manifestation of a liquid-gas phase transition. Therefore, if this picture is correct, the proton-induced heavy-ion collision creates a hot nuclear system, expands until the critical point is reached, where then undergoes an abrupt transformation from the liquid state (expanded nucleus) to a gaseous state (gas of fragments). This is in essence the liquid-gas phase transition model.

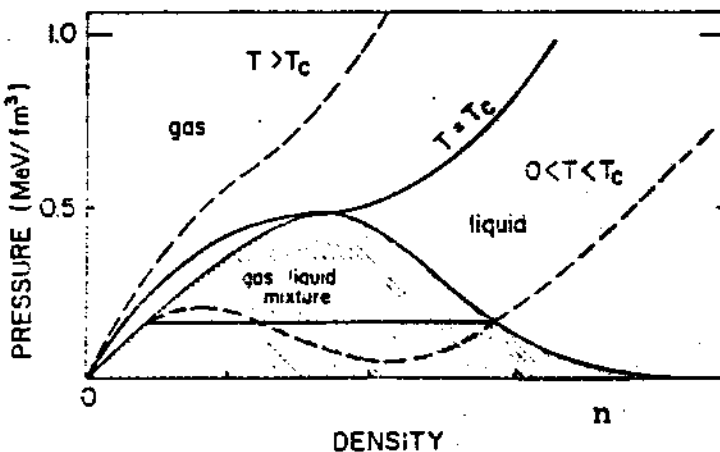
This interpretation for nuclear fragmentation received

several supports from the theory (e.g., Jaqaman, Mekjian and Zamick, 1983; Panagiotou, Curtin and Scott, 1985) and is strongly based on the power-law. However, the analogies mentioned above can not be pushed too far, simply because the same law may not imply the same physics. In effect, Hüfner and Mukhopadhyay (1986) reported the mass distribution of the fragments resulting from the collisions between two basalt stones as $m^{-1.68}$ and, in the case of asteroids in our planetary system as $m^{-1.7}$. Of course, it is hard to believe that these phenomena and the nuclear fragmentation share the same physics. So, the liquid-gas phase transition model provoked much controversy and received criticisms.

However, before discussing briefly these criticisms, let me recall some simple ideas about phase transition and phase equilibrium in a van der Waals-type system (Landau and Lifshitz, 1964).

It was mentioned that in the Hartree-Fock approximation the nuclear matter has a similar behaviour than a van der Waals gas. In the phase diagram pressure x number density

(Fig. 11), the critical point is defined by $(\frac{\partial P}{\partial n})_T = (\frac{\partial^2 P}{\partial n^2})_T = 0$



such that, for $T > T_c$ and $P > P_c$, the system is always homogeneous. For $T < T_c$ and $n < n_c$, homogeneous states are unstable against the phase separation.

FIG. 11 - Taken from Bondorf et al. (1985a).

The phase equilibrium requires equality of the pressure and the chemical potentials of the two phases, and this is usually accomplished through a Maxwell construction of equal areas. The locus of the transition points is the Maxwell curve (coexistence curve). Under this curve, the gas state and the liquid state can be found in phase equilibrium.

It is displayed in Fig. 12 the isothermal spinodal, defined as the locus of points satisfying $(\frac{\partial P}{\partial n})_T = 0$, and similarly the isentropic spinodal, given by $(\frac{\partial P}{\partial n})_S = 0$. The area between the Maxwell curve and the isothermal spinodal defines the region in which a superheated liquid or a supercooled vapour may exist. It is the region of metastability for single phase. Under the isothermal spinodal, the system is unstable as a homogeneous body in any state, i.e., neither uniform liquid nor uniform gas is stable.

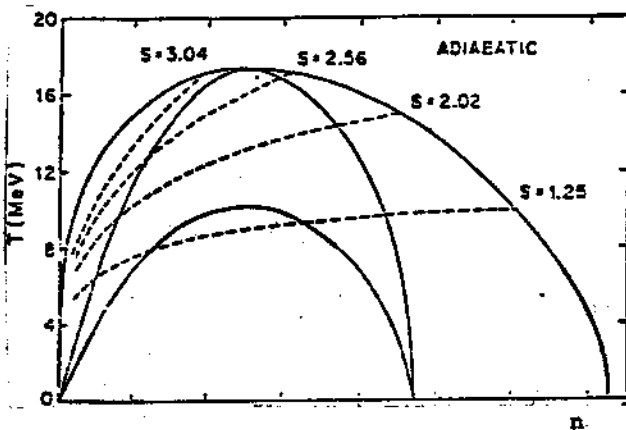


FIG. 12 - Taken from Glendenning (1986).
side ($n < n_c$, $T < T_c$), then droplets begin to form in the gas.

Next consider a hot nuclear system which expands and cools. If the system reaches the coexistence curve on the higher density side ($n > n_c$, $T < T_c$), then bubbles will be found in the liquid. If it hits on the low density

Let me come back to the criticisms concerning the liquid-gas phase transition model. The main criticisms are the following:

Schlagel and Pandharipande (1987), using classical molecular dynamics, have shown that in a 108+108 reaction (solid lines in Fig. 13) and 65+65 reaction (dashed lines), the instabilities develop far from the critical point. Boal (1984) complains that the nuclear region involved in proton-induced

reactions is both too small and too short-lived to support a sharp transition. Furthermore, Aicheilin et al. (1988) have simulated Ne (1.05 GeV/n) + Au reaction, via microscopic quantum molecular dynamics and found that the

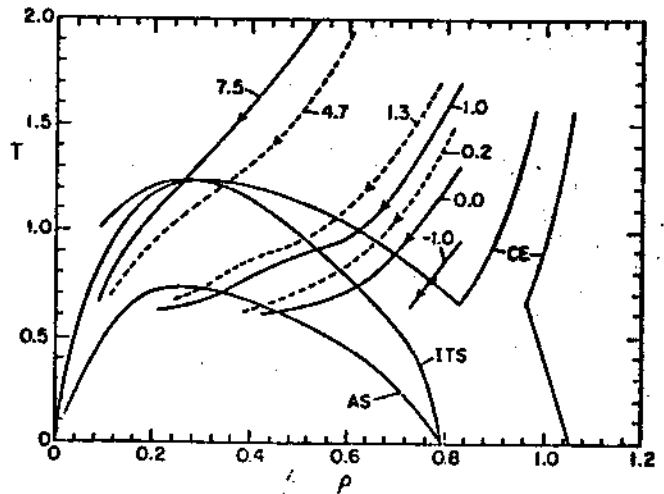


FIG.13 - Taken from Schlagel and Pandharipande (1987).

mass yield is given by a power-law, but that the power-law shape is caused by simply averaging over different impact parameters. They conclude that this fact rules out inclusive mass distribution as a signature of a liquid-gas phase transition.

Last, but not least, a simple question may be made: Why is one so lucky in obtaining through a heavy-ion collision with so many different initial states, a trajectory in the phase diagram that hits exactly on the critical point ?

4.2 - Statistical Multifragmentation Model

This model is proposed by Bondorf et al. (1985a, 1985b). They consider a portion of expanding hot nuclear matter, just in the verge to disassembly. The model assumes the following picture


-22-

of the fragmentation process: a) production of a hot matter and appearance of cracks; b) explosive formation of primary fragments; and c) evaporation of particles from primary fragments. Also, it is assumed that at the break-up stage, the system is characterized by mass number A_0 , charge Z_0 , volume V_0 and total energy E_0 .

One basic hypothesis is that the system attains the thermalization just before the break-up. This means that the reaction time is assumed greater than both the temperature equilibration time and the composition equilibration time. In consequence, both the temperature T and the average composition of the fragments can be regarded as essentially constant throughout the entire volume of the system.

Let's consider the initial hot nuclear system (Z_0, A_0) to split into different fragments with mass number A , charge Z and energy $E_{Z,A}$. The number of (Z,A) fragments is denoted by $N_{Z,A}$. Let's introduce the partition vector $\{N_A\}$, where $N_A = \sum_Z N_{Z,A}$. For example, the partition in which a nucleus $A_0 = 10$ splits into 2 single nucleons and 2 alfa particles, is represented by

$$\{N_{10}\} = (2, 0, 0, 2, \dots, 0)$$



10 components

The total fragment multiplicity is

$$M = \sum_A N_A \quad . \quad (14)$$

The problem of partitioning a finite particle system

into several fragments is formally identical to one of decomposing a given integer number into integer terms. The number of partitions of a system with A_0 nucleons is given by

$$P(A_0) = \sum_{M=1}^{A_0} P(A_0, M) \quad (15)$$

where

$$P(A_0, M) = \sum_{0 \leq K \leq \frac{A_0}{M} - 1} P(A_0 - KM - 1, M - 1)$$

Note that for $A_0 = 100$, the total number of partitions is $\approx 2 \times 10^8$.

The statistical multifragmentation model is based on a microcanonical approach, where mass, charge and energy are fixed, but the coarse graining approximation is used, i.e., state subsets of the system are replaced by its mean values. In this case, the subsets are represented by the excited states of each nucleus.

The partitions are required to satisfy to very general conservation laws:

a) baryon number conservation

$$A_0 = \sum_{Z, A} N_{Z, A} A \quad (16)$$

b) charge conservation

$$Z_0 = \sum_{Z, A} N_{Z, A} Z \quad (17)$$

c) energy conservation

$$E_{\text{total}} = E_0^* + E_0^{\text{GS}} = \frac{3}{5} \frac{Z_0^2 e^2}{R_D} + \sum_{Z, A} N_{Z, A} E_{Z, A} \quad (18)$$

where E_0^{gs} is the ground-state energy of the initial system and R_b is related to the volume $V_b > V_0$ at the break-up. The Coulomb energy of a homogeneous charged sphere has been projected out from the total energy for computational convenience.

Then, as usual, the partitions are assumed to have statistical weights given by

$$W(\{N_A\}) = \exp[S(\{N_A\}, T, V_b)] \quad (19)$$

where:

$$S(\{N_A\}, T, V_b) = \sum_{Z,A} N_{Z,A} S_{Z,A}(T, V_b)$$

In order to calculate $S_{Z,A}$, a generalization of the liquid drop model to finite temperature is required. It is assumed that only the surface and bulk terms are modified.

As a matter of fact, the surface free energy is parametrized according with Ravenhall et al. (1983), as

$$F_A^S(T) = \beta(T) A^{2/3} = \beta_0 \left(\frac{T_C^2 - T^2}{T_C^2 + T^2} \right)^{5/4} A^{2/3} \quad \begin{array}{l} T < T_C \\ T \geq T_C \end{array}$$

$$= 0 \quad (20)$$

where $\beta_0 = 18$ MeV.

The bulk free energy is given by

$$F_A^{bulk}(T) = (W_0 - \frac{T^2}{\epsilon_0}) A \quad (21)$$

where T^2/ϵ_0 takes into account the effect of the excitation in the bulk energy, and $W_0 = -16$ MeV and $\epsilon_0 = 16$ MeV.

The symmetry and Coulomb contributions to the free

energy are, respectively,

$$F_{Z,A}^{\text{sym}} = \gamma \frac{(A-2Z)^2}{A}, \quad \gamma = 25 \text{ MeV} \quad (22)$$

$$F_{Z,A}^{\text{C}} = \frac{3}{5} \frac{Z^2 e^2}{R_{Z,A}} [1 - (1+\chi)^{-1/3}] \quad (23)$$

with

$$\chi = [1 + \frac{d}{R_0} (M^{1/3} - 1)]^3 - 1,$$

where $R_0 = 1.17 A_0^{1/3}$ and $2d = 2.8 \text{ fm}$. $2d$ is the crack width and is estimated as the separation between surfaces of spherical nuclei, in which the Coulomb repulsion is counterbalanced by nuclear forces.

Let's now to calculate the free energy for a fragment (Z,A) . First, it should be noted that the total partition function can be factorized into translational and internal components, if it is assumed no interaction among fragments, i.e.,

$$Z_{Z,A} = Z_{Z,A}^{\text{transl}} \cdot Z_{Z,A}^{\text{int}}$$

Furthermore, in the case of subsystem composed of $N_{Z,A}$ identical fragments, the partition function is

$$\frac{(Z_{Z,A})^{N_{Z,A}}}{N_{Z,A}!}$$

$Z_{Z,A}^{\text{transl}}$ is obtained by integrating over the whole available phase space, i.e.,

$$Z_{Z,A}^{\text{transl}} = g_{Z,A} V_f \left(\frac{m_{Z,A} T}{2\pi\hbar^2} \right)^{3/2} \quad (24)$$

where $g_{Z,A}$ is the spin degeneracy factor,

$m_{Z,A} \approx m_N A$ (m_N = nucleon mass) and $V_f = V_b - V_0 = \chi V_0$ is the free volume.

As $F = T \ln Z$, we can also decompose the free energy into translational and internal terms,

$$F_{Z,A} = F_{Z,A}^{\text{transl}} + F_{Z,A}^{\text{int}}$$

with:

$$F_{Z,A}^{\text{transl}} = -T \left[\ln Z_{Z,A}^{\text{transl}} - \frac{1}{N_{Z,A}} \ln N_{Z,A} \right] \quad (25)$$

$$F_{Z,A}^{\text{int}} = (W_0 - \frac{T^2}{\epsilon_0}) A + \beta(T) A^{2/3} + \gamma \frac{(A-2Z)^2}{A} + \frac{3}{5} \frac{Z^2 e^2}{R_{Z,A}} [1 - (1+\chi)^{-1/3}] \quad (A > 4) \quad (26)$$

Since $S_{Z,A} = - \left(\frac{\partial F_{Z,A}}{\partial T} \right)_V$, then

$$S_{Z,A} = \ln(g_{Z,A} \frac{\chi V_0 A^{3/2}}{\Lambda^3}) - \frac{1}{N_{Z,A}} \ln N_{Z,A} + \frac{2T}{\epsilon_0} A - \frac{d\beta}{dT} A^{2/3} + \frac{3}{2} \quad (A > 4) \quad (27)$$

where $\Lambda = \left(\frac{2\pi\hbar^2}{m_N T} \right)^{1/2}$ is the nucleon thermal wavelength.

Once $S_{Z,A}$ is put in the equation defining $W(\{N_A\})$, the expectation value of any quantity X is

$$\bar{X} = \sum_{\{N_A\}} W(\{N_A\}) X(\{N_A\}) \quad (28)$$

where $X(\{N_A\})$ is the value of X for the partition $\{N_A\}$, and the sum is over all possible partitions of the system.

As a direct calculation of this equation is very difficult due to the large number of possible partitions (remember that in the case of $A_0 = 100$, the number is $\sim 2 \times 10^8$), some approximation scheme has to be used. One possible approximation is the Monte Carlo procedure. In the following we describe the main steps:

1. A multiplicity M is randomly chosen, according with a distribution proportional to the relative number of partitions with multiplicity M ;
2. A random partition is obtained. The charges of the fragments are then attributed, assuming approximation of beta-stable nuclei;
3. For a given input (A_0 and E_0^*/A_0), the temperature of the gas of the fragments is determined by solving the equation of energy conservation. If it happens that this conservation is not satisfied for any $T > 0$, then the partition is dropped and a new partition is tried;
4. With $\{N_A\}$ and T known, the entropy $S(\{N_A\})$ and the probability $W(\{N_A\})$ are computed;
5. The quantity X is evaluated and the corresponding expectation value is computed by Eq. (28);
6. The procedure is repeated again and again, until satisfactory statistic is obtained.

In the following, we present the main results from the statistical multifragmentation model for $A_0 = 100$. In Fig. 14, the average multiplicity \bar{M} is plotted against excitation energy per particle E^*/n . It is seen that \bar{M} maintains equal 1 up $E^*/n \approx 3$ MeV, when the fragmentation begins and, after

that, increases steadily with increasing E^*/n . In Fig. 15, the average temperature \bar{T} is also given as function of E^*/n . In this plot, it is clear that, instead one, two phase changes are found. The first one occurs at $T \approx 6$ MeV and E^*/n around 3-4 MeV and corresponds to the nuclear fragmentation, whereas the second one is observed at $T \approx 10$ MeV and E^*/n around 16 MeV and corresponds to an equivalent liquid-gas phase transition at the critical temperature of the infinite nuclear matter.

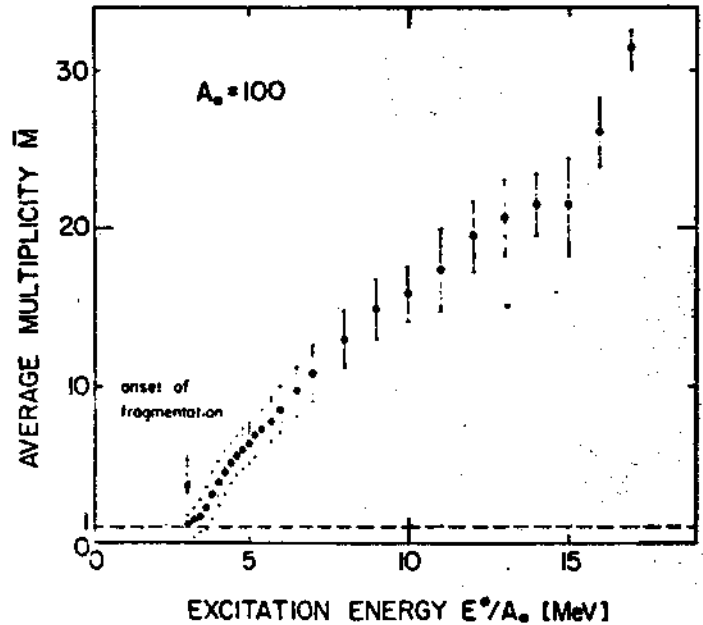


FIG. 14 - Taken from Bondorf et al. (1985b).

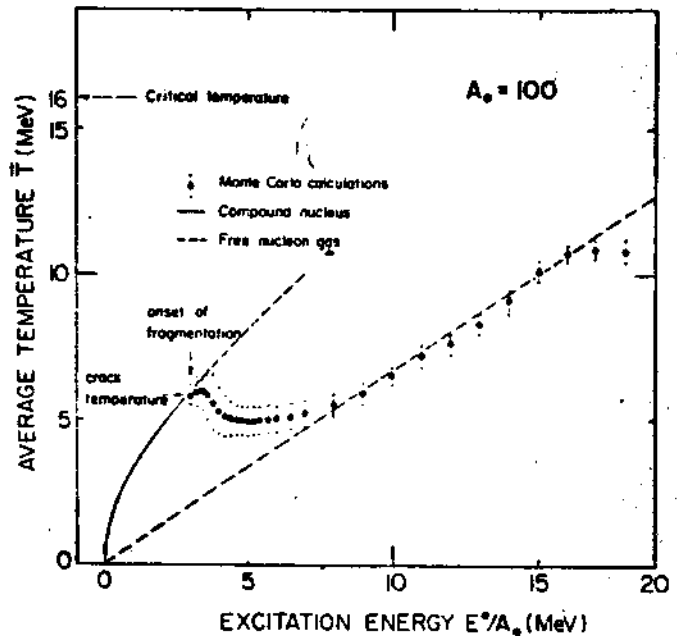


FIG. 15 - Taken from Bondorf et al. (1985b).

The average fragment

multiplicity \bar{N}_A is plotted in Fig. 16 against the fragment mass number A for $E^*/n = 4.0$ MeV. This result should not be compared with experimental data, since it does not incorporate secondary evaporation processes.

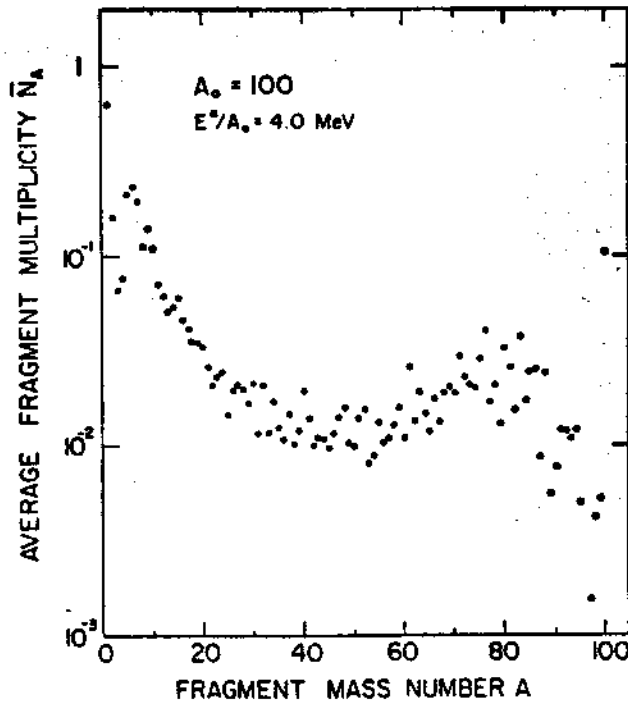


FIG. 16 - Taken from Bondorf et al. (1985b).

4.3 - Cold Fragmentation

Let me now introduce briefly a reaction mechanism for nuclear fragmentation which is appropriate to high energy heavy-ion-induced collisions. It is proposed by Aichelin, Hüfner and Ibarra (1984).

At high-energy nucleus-nucleus collision ($> 500 \text{ MeV/n}$), the exchanged transverse momentum is small (typically $\sim 0.4 \text{ GeV/c}$). This means that for a large longitudinal momentum, we have small scattering angles, i.e., the nucleons move almost on straight lines. Then, after the collision, we find (Fig. 17):

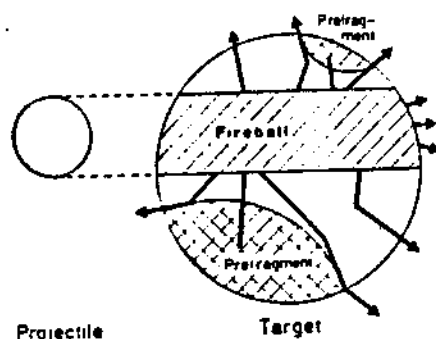


FIG. 17 - Taken from Aichelin et al. (1984).

- a) a participant region, formed by nucleons which have undergone scatterings. Essentially this region is given by the geometrical overlapping between projectile and target nuclei;
- b) a spectator region, formed by nucleons outside the overlapping. These nucleons are unscattered and the matter is relatively cold.

In the participant region, the most part of the beam energy is converted into heat. High temperatures are reached, and the region is close to thermal equilibrium. It uses to say that it behaves as a fireball.

It is clear also that the target spectator is almost at rest, and the projectile spectator moves with approximately the beam velocity. It is within this participant-spectator picture that the cold fragmentation model is proposed.

The relevant feature of this model is that it does not assume thermodynamical equilibrium. According to this model, nuclear fragmentation is regarded as the shattering of a glass, when hit by a stone. This picture is compatible with nuclear fragmentation as arising from a mechanical instability.

The nuclear fragmentation is treated by this model as a two-step process:

- a) Formation of the participant and the spectator regions, with the former giving a fireball and the latter forming a cold matter;
- b) The fireball decays. Some participants escape without any further collision, others penetrate into the spectator region and deposit momentum and energy. This leads to local instabilities, which destabilizes globally the spectator matter.

Then, Coulomb forces act on the pieces (prefragments) pushing them apart. Secondary decays (evaporation) may occur before they are detected as fragments.

The model ascribes a following parametrization to the triple differential cross section,

$$\frac{d\sigma^3}{dE d\Omega dZ} = \frac{d\sigma}{dZ} (Z, s, \sigma_F) \int_0^{V_C^{\max}} dV_C g(V_C) f(E, \Omega, v_{cm}, P_{||}, \Delta, V_C) \quad (29)$$

In Eq. (29), $d\sigma/dZ$ is the charge yield curve and gives the distribution of "cracks" in the target spectator; $g(V_C)$, the Coulomb barrier distribution, taking into account the different places in the target that the clusters can be formed; $f(E, \Omega, v_{cm}, P_{||}, \Delta, V_C)$, the energy and angle distribution for a given value of the Coulomb barrier.

In order to calculate $d\sigma/dZ$, it was used the principle of minimum information (Aichelin and Hüfner, 1984). In fact, assuming all partitions to be equally probable, the shape of the charge yield is given by

$$\frac{d\sigma}{dZ} = \sigma_F [\exp(1.28 z/\sqrt{Z_0}) - 1]^{-1} \quad (30)$$

where Z_0 is the charge of the spectator matter and σ_F is the integrated cross section for fragmentation of the target.

One criticism which can be made to this model is that Eq. (30) represents actually a Bose-Einstein distribution. This means that, in the cold fragmentation model, all nuclear fragments are treated as if they were bosons, but this is true only in the case of an even number of nucleons.

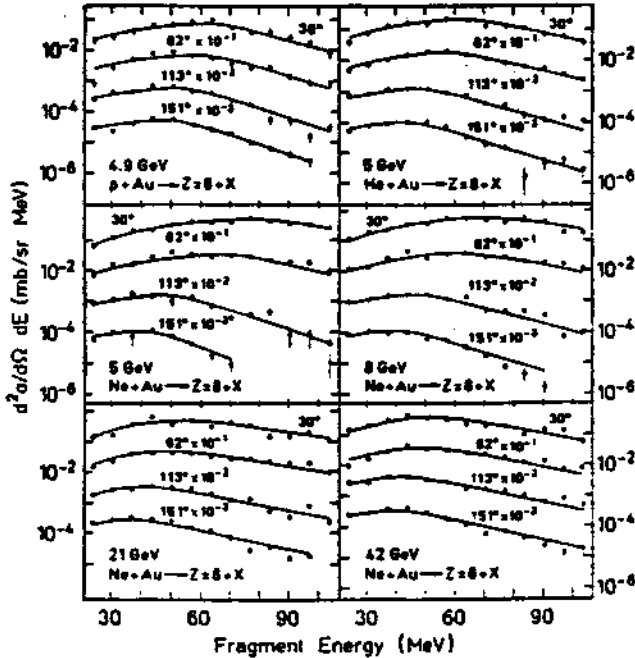


FIG.18 - Taken from Aichelin et al. (1984).

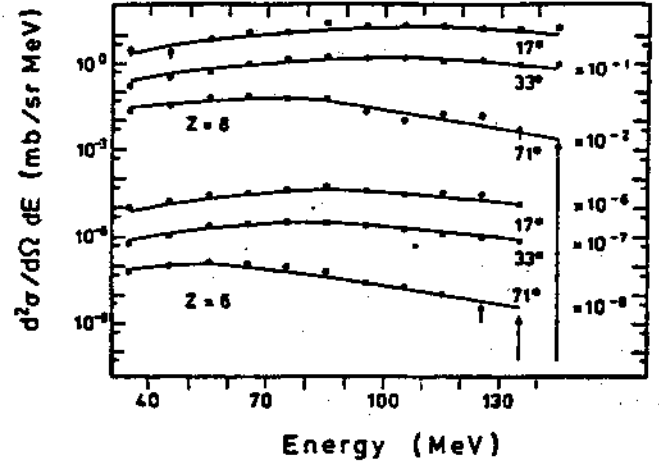


FIG. 19 - Taken from Aichelin et al. (1984).

Figs. 18 and 19 show the results of the fitting for $d^2\sigma/d\Omega dE$ (solid line) in comparison with the data taken from Warwick et al. (1983) and for Bock et al. (1982), respectively. In this latter case, the reactin is $^{16}\text{O}+\text{Au}$ (top curves) and $^{12}\text{C}+\text{Au}$ (botton curves), both at 84 MeV/n of bombarding energy.

4.4 - Sequential Evaporation

One model which does not assume a simultaneous break-up is given by the sequential evaporation model, proposed by Friedman and Lynch (1983a). This model treats nuclear fragmentation as a number of evaporation processes in succession, i.e, the compound system, assumed in thermal equilibrium, evaporates a particle, and after thermalization, evaporates another particle and this process is repeated again and again, until

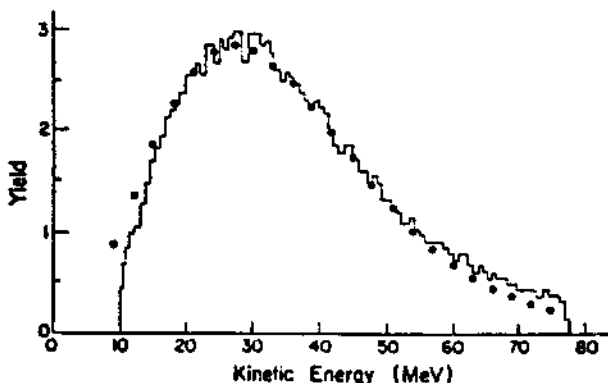
the fragment excitation energy is reduced to values below the evaporation threshold.

Formally, the evaporation process is treated as a statistical emission. An expression for the rate of emission is worked out as a generalization of the evaporation of a Fermi gas from a spherical well. Specifically, if n_a denotes the number of emitted clusters of type a , with number of protons Z_a and number of neutrons N_a , the rate of emission at temperature T of clusters of type a with energy between E and $E+dE$, is given by

$$\frac{d^2N}{dEdt} = (2S_a + 1) \left(\frac{m_a - R_a^2}{\pi \hbar^3} \right) (E - V_a) \theta(E - V_a) \exp\left(-\frac{E}{kT}\right) \times \exp\left\{\frac{1}{kT} [Z_a f^*(T, \rho_p) + N_a f^*(T, \rho_n) - B_a]\right\} \quad (31)$$

where S_a , m_a , R_a and B_a are, respectively, the spin, mass, radius and separation energy of the cluster a . V_a represents the Coulomb barrier and f^* , the reduced free excitation energy, which is a function of the number density of protons ρ_p or of neutrons ρ_n . $\theta(x)$ is the step function.

The recoil of the residual nucleus can be also easily taken into account. For details, we refer the reader to the



reference given above.

FIGURE 20 - Taken from Friedmann and Lynch (1983b).

In Fig. 20, we show the energy spectrum of ^{12}C from ^{132}Xe for $T = 15$ MeV. The dots denote the results obtained from sequential evaporation and the histogram, the experimental data from Finn et al. (1982). The agreement is very nice, but the temperature used in the fitting is very high and the corresponding excitation energy per particle (11 MeV) is much higher than the maximum value (~ 6 MeV) experimentally observed (see Leray, 1986). Fig. 21 displays the calculated mass yield (dots) and the data (solid line) from Finn et al. (1982). Fig. 22 gives the isotopic yield from ^{132}Xe for isotopes of C (solid line), N (dashed line) and O (dot-dashed line).

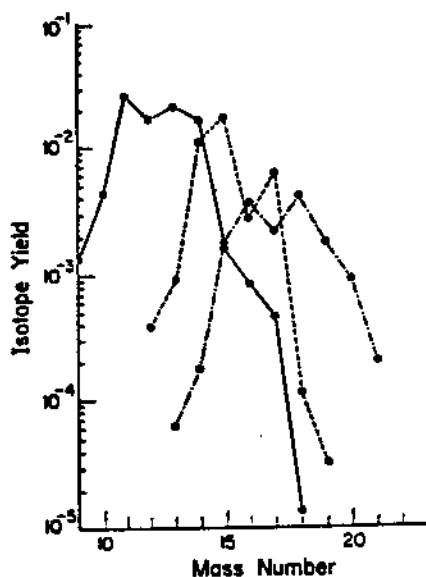


FIGURE 22 - Taken from Friedmann and Lynch (1983b).

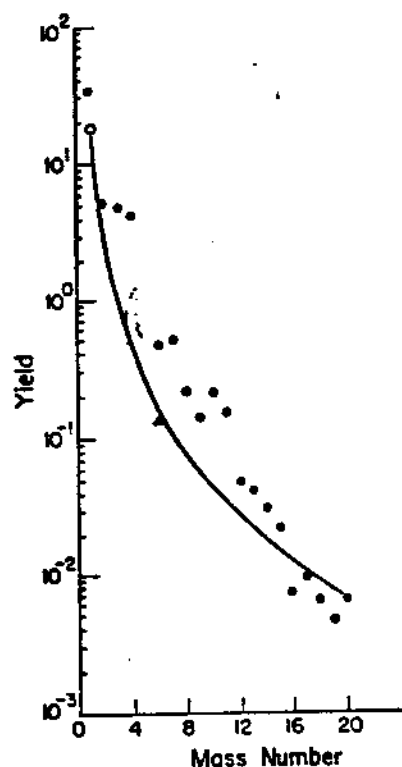


FIGURE 21 - Taken from Friedmann and Lynch (1983 b).

V. UNIFORM EXPANSION APPROXIMATION AND ENERGY SPECTRA

In order to extract informations from their experimental data, Hirsch et al. (1984) have used the fragment kinetic energy data for evaluating the location at which the fragment was produced inside the nuclear system. In the following, we will discuss how this can be accomplished.

Consider a remnant of the proton-induced reaction with radius R_0 . A fragment of radius r is assumed to be formed at a distance R from the center of the remnant (fig. 23). For

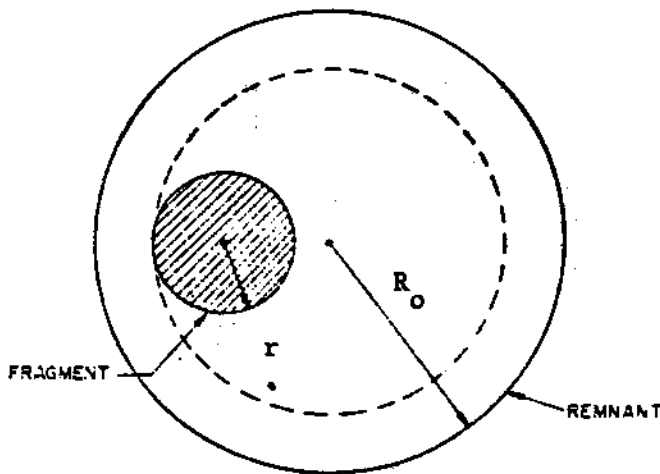


FIGURE 23

simplicity, it is assumed that the fragment interdistances are changed in the same way as the radius of the system (uniform expansion). This means that a charge which initially is outside a sphere of radius R will stay outside during the

whole expansion process, and vice-versa. In consequence, the charges outside the sphere of radius R will have no influence on the Coulomb repulsion energy of the fragment.

In the uniform expansion, the final kinetic energy of the different fragments is

$$E_k^{\text{final}} = E_k^{\text{initial}} + E_{\text{Coul}}^{\text{break-up}}$$

Therefore, the Coulomb energy of the fragment (Z,A) is given by

$$E_{\text{Coul}} = \frac{ZZ_0 e^2}{R_0^3} (R^3 + 3rR) \left(1 - \frac{A}{A_0}\right)^2 \quad (32)$$

where Z_0 , A_0 refer to the remnant and the last factor is included in order to take into account the momentum conservation.

Solving this equation for R , we obtain

$$R(E_{\text{Coul}}) = \frac{1}{2} (9r^2 + 4C)^{1/2} - \frac{3}{2} r \quad (33)$$

where

$$C = \frac{R_0^3}{ZZ_0 e^2 \left(1 - \frac{A}{A_0}\right)^2} E_{\text{Coul}}$$

Assuming E_k^{initial} very small, such that

$$E_k^{\text{final}} = E_k \approx E_{\text{Coul}}$$

and putting experimental values of E_k (peak values) in the above equation, it is obtained a correlation between the fragment size and the location where the fragment is most likely be formed inside the remnant. Effectively, in fig. 24, fragment location is plotted versus the fragment mass A for $p+Kr$ (a) and $p+Xe$ (b) reactions. It is clear that the larger fragments are formed closer to the center of the remnant.

However, it is noted that the expression for E_{Coul} was derived by assuming implicitly that the fragment radius also increases during the expansion in the same way than the rest of the system. This assumption is clearly unreasonable and may produce large systematic error, mainly in the case of large fragments.

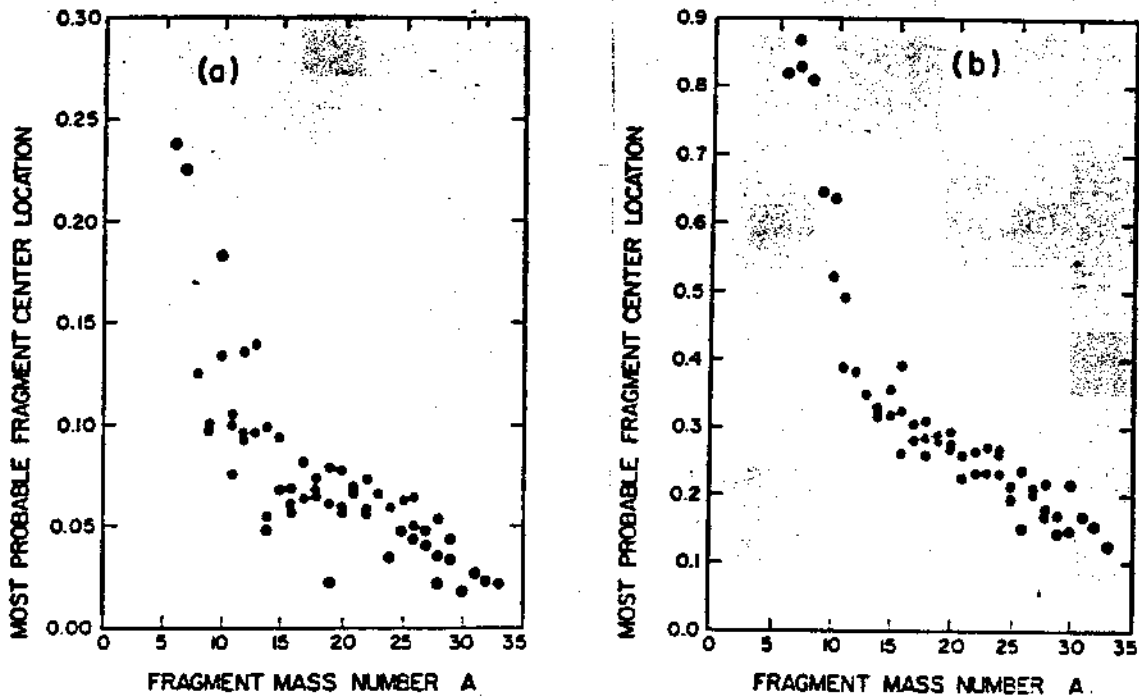


FIGURE 24 - Taken from Hirsch et al. (1984).

In order to clarify this point, Chung, Donangelo and Schechter (1987) have proposed a modification to the uniform expansion of Hirsch et al., by assuming the fragment radius fixed at its initial value as the expansion proceeds. In consequence, the remaining charge distribution develops a hole around the fragment. Under this assumption, the kinetic energy due to Coulomb repulsion is

$$E_{\text{Coul}} = \frac{ZZ_0 e^2}{R_0^3} R^2 \left(1 - \frac{A}{A_0}\right)^2 \quad (34)$$

which does not contain the term $3 R r$ of Eq. (32). Since this term may give important contribution, Eq. (32) is expected to overestimate the fragment kinetic energies.

It should be noted that in the uniform expansion approximation, $E_{\text{Coul}} = f(R)$, where R is the location of the fragment at the beginning of the expansion.

However, at the break-up, the fragments already have thermal velocities. So, their relative velocities are expected to shift during the expansion. As these initial velocities depend on the average temperature and the fragment masses, the deviations from Eq. (34) are expected to depend on the total energy of the system as well as on the mass of the particular fragment which spectrum is being considered.

In order to make comparisons with the results predicted by the new assumption, Chung et al. (1987) have performed a dynamical calculation, using the statistical multifragmentation model to describe the break-up process. At the break-up, it is assumed that the fragments are sufficiently separated, so that only Coulomb forces must be considered.

To obtain a dynamical description of the Coulomb expansion, it is assumed the following classical Hamiltonian,

$$H = \sum_i \frac{p_i^2}{2m_i} + \sum_{i < j} \frac{z_i z_j e^2}{|\vec{r}_i - \vec{r}_j|} \quad i = 1, \dots, M \quad (35)$$

The coupled differential equations of motion are obtained from this Hamiltonian and then integrated numerically. A Monte Carlo procedure is used to produce average values of the physical quantities. The positions \vec{r}_i are randomly selected from a uniform spherical distribution, and the \vec{p}_i are obtained from the Maxwell-Boltzmann distribution associated to the excitation energy of the system. The time evolution of the Coulomb expansion process is stopped when the total energy of each fragment ceases to display appreciable changes. These final total energies are then stored and the procedure repeated.

They have calculated the energy spectra for ^{12}C for different excitation energy per particle. The results are displayed in Fig. 25. It is seen that the spectra calculated with

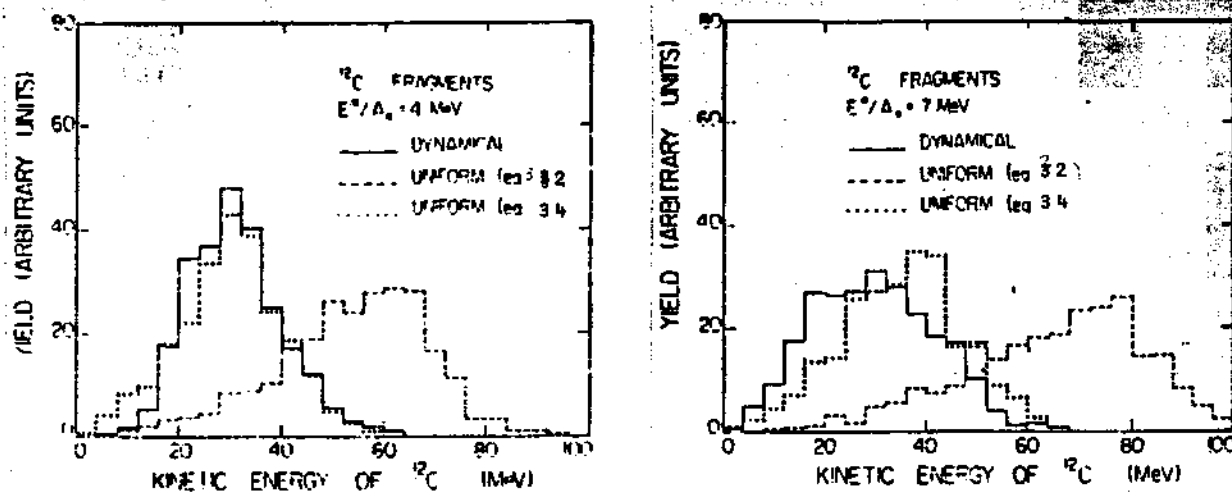


FIGURE 25 - Taken from Chung et al. (1987).

Eq. (34), using the new assumption, are quite different from the calculated with Eq. (32) and are closer to the experimental results, in spite of the fact that the secondary evaporation was not taken into account.

VI. PERCOLATION MODELS

6.1 - Percolation Background

It seems to be worthwhile to give some background in the percolation theory, before to discuss percolation models. Let me begin with some historical notes:

1940 - Flory and Stockmayer (study of molecules growing)

1957 - Broadbent and Hammersley (coined the name and gave an initial mathematical formalism)

1971 - Emphasis on critical phenomena

Nowadays, the percolation theory has wide-spread applications, e.g., gelation of polymers in condensed matter, study of the plasma quark-gluon (Baym, 1979; Ngô et al., 1988), spread of fires in forests, propagation of disease in plantations, and many others. The reader interested in percolation theory will find useful the following references: Essam (1980), Kirkpatrick (1973) and Stauffer (1985).

We introduce now the basic ingredients of the theory, i.e:

- 1) A distribution of a collection of points in a d -dimensional space. For simplicity, a regular lattice is used and, in this case, the points are the lattice sites.
- 2) A criterion for deciding whether two given points are connected or not. Subsets of connected points are called clusters and the study of the properties of these clusters constitutes the percolation theory.

The main types of percolation are the following:

- a) Bond Percolation, in which all sites are occupied and each bond can be broken with probability p_B or unbroken with probability $1 - p_B$, where $0 \leq p_B \leq 1$.
- b) Site Percolation, in which all bonds are unbroken and each site has probability p to be occupied or $1-p$ to be unoccupied, with $0 \leq p \leq 1$.

A hybrid percolation is also possible and is given by the site-bond percolation. In this case, the sites of the bond percolation are no longer all occupied; only a fraction of

sites is occupied. Bonds between neighboring occupied sites are unbroken with probability $1 - p_B$.

One important quantity in the percolation theory is the percolation threshold p_c , which is defined as the concentration p at which an infinite network (percolation cluster) appears in an infinite lattice, so that for $p \geq p_c$, one has a cluster extending from one side of the system to the other (percolating cluster); and for $p < p_c$, no such infinite cluster exists. In Table 1, percolation thresholds are listed for several types of lattice, both for bond and site percolation.

TABLE 1 - Taken from Stauffer (1985).

LATTICE	SITE	BOND
Honeycomb	0.6962	0.65271
Square	0.59275	0.50000
Triangular	0.50000	0.34729
Diamond	0.428	0.388
Simple cubic	0.3117	0.2492
BCC	0.245	0.1785
FCC	0.198	0.119

However, it should be noted that in actual lattices, finite-size effects will modify somewhat this result. Instead a sharp transition from non-percolating regime to percolating regime, it is observed a smoother transition with a width that is related to finite-size effects, such as it is exemplified in Fig. 26, taken from Bauer et al. (1986). In this figure, the ordinate represents the probability for the formation of a percolating cluster p_{perc} and the abscissa, the breaking probability for bond percolation p_B . The curves are results of a simulation on simple cubic lattice with n^3 sites.

Let me now remind that percolation theory is concerned with the properties of the clusters. So, if n_s denotes the number of cluster of size s per lattice site, the first step is to obtain the function $n_s = f(p,s)$, where p is the probability. The second step is to study its properties, mainly for $p \rightarrow p_c$.

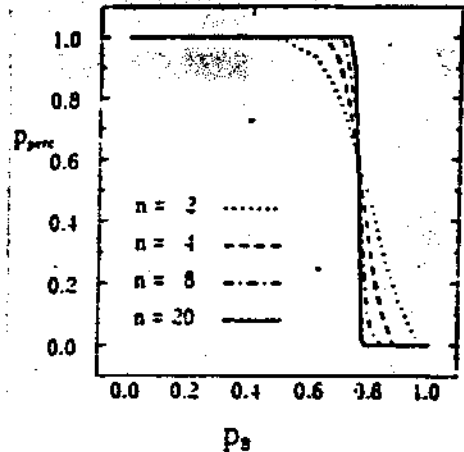


FIGURE 26 - Taken from Bauer et al. (1986).

Now, we summarize the main results of the percolation theory, such as given in Stauffer (1985). In this discussion, only infinite lattices are considered. For simplicity, we begin with simple cases, where exact solution does exist (one dimension and Bethe lattice). First, we consider the one-dimensional lattice.

In this simplest case, the "lattice" is just an infinitely long linear chain of points, placed in fixed and equally spaced distances. If p is the probability for each site to be occupied, simple probabilistic arguments give

$$n_s = p^s (1 - p)^2 \quad . \quad (36)$$

In Eq. (36), for $p < 1$, $n_s \propto \exp(-s)$ if $s \rightarrow \infty$.

In this one-dimensional lattice, for $p = 1$, all sites are occupied and we have only one single cluster. For every $p \neq 1$, the percolation cluster will fail to exist, since in this case at least one hole will be found in the chain. Therefore, $p_c = 1$, and we have, in one dimension, only the region $p < p_c$.

This means: no phase transition in one-dimensional percolation problem.

It is useful to define the mean cluster size,

$$S = \frac{\sum_s n_s s^2}{\sum_s n_s s} \quad (37)$$

or, according with Eq. (36),

$$S = (1+p)/(1-p) \quad p < p_c \quad (38)$$

Therefore, in one dimension, S diverges at the critical probability.

Next, we consider the Bethe lattice which also presents an exact solution. Bethe lattice is a structure in which from each site come out z other neighboring sites, in a ramifying way.

In this case, the percolation threshold is $p_c = 1/(z-1)$ and the mean cluster size (hereafter the case of $z = 3$ is assumed) is

$$S = p(1+p)/(1-2p) \quad , \quad p < p_c \quad (39)$$

Furthermore,

$$n_s(p)/n_s(p_c) \propto \exp(-cs) \quad , \quad (40)$$

where $c \propto (p-p_c)^2$ with $p \rightarrow p_c$, and $n_s(p_c)$ is given by the Fisher droplet model as $n_s(p_c) \propto s^{-\tau}$, for large s ($\tau = 5/2$ in the Bethe lattice).

With relation to n_s , an attempt to generalize for d -dimensional case the formulae derived in one-dimensional and

Bethe lattices is

$$n_s \propto s^{-\tau} \exp(-cs) \quad , \quad s \rightarrow \infty \quad , \quad (41)$$

with $c \propto |p-p_c|^{1/\sigma}$, $p \rightarrow p_c$ and σ is another critical exponent.

However, the one-dimensional result does not fit in this generalization, because from Eq. (36),

$$n_s(p) = (p_c - p)^2 \exp[-(p_c - p)s] \quad , \quad p \rightarrow p_c \quad (42)$$

we have a power of $(p-p_c)$ instead a power of s . What to do ? Keep the one-dimensional result ? Or the Bethe lattice result ?

It seems that the last alternative is more reasonable, because the Bethe lattice presents at least a percolative phase transition ($p_c < 1$).

One possible modification is to drop the combination

$$z = cs \propto |p-p_c|^{1/\sigma} s$$

in favour of

$$z \propto (p-p_c) s^\sigma \quad .$$

In this case,

$$n_s(p) = n_s(p_c) \exp(-z)$$

where $n_s(p_c) = s^{-\tau}$, or:

$$n_s(p) = s^{-\tau} \exp[-\text{const} \times (p-p_c) s^\sigma] \quad . \quad (43)$$

But, this expression is somehow similar to the previous assumption

$$n_s(p) = s^{-\tau} \exp[-\text{const } |p-p_c|^{1/\sigma} s] \quad (44)$$

In fact, both expressions depend on two variable, s and $(p-p_c)$, through the combination $|p-p_c| s^\sigma$ only. Therefore, we arrive to the scaling function

$$n_s = s^{-\tau} f[(p-p_c)s^\sigma] \quad , \quad p \rightarrow p_c \quad , \quad s \rightarrow \infty \quad (45)$$

The precise form of the scaling function $f[(p-p_c)s^\sigma]$ has to be determined by computing calculations and no deviations from this scaling assumption has been detected (at least, yet) for conventional percolation in two and three dimensions. Note that $f(0) = 1$.

From Eq. (45), we obtain a power law for n_s in the case of $p \rightarrow p_c$.

It is important to define the moments M_k of the distribution n_s , i.e:

$$M_k = \sum_s s^k n_s \quad (46)$$

where the sum has to be understood to exclude the infinite cluster.

After this digression in percolation theory, let me discuss the percolation models for nuclear fragmentation.

6.2 - Percolation Approach for Nuclear Fragmentation

The percolation approach for nuclear fragmentation is based on the assumption that the nucleon configuration inside the nucleus can be described by a lattice. This should cause no emba-

rassment since, in the range this approach is supposed to hold, the nucleon Fermi motion can be neglected.

The most part of the percolation models are concerned mainly with the way of how to generate and identify clusters. In what follows, only site percolation is used, unless the contrary is explicitly assumed.

The procedure to generate clusters may be the following:

- a) Choose a lattice (the simplest one is the cubic simple, but other lattices also can be used as the fcc and the bcc), containing A_0 sites;
- b) If the site probability is p , then the number of occupied sites (= nucleons) is $A = pA_0$.
- c) Allocate randomly these A nucleons into A_0 sites;
- d) Look for all subsets (clusters) formed by connected nucleons and collect them according with its size. The conventional definition of clusters requires only connection via nearest-neighborhood distance, such is illustrated in Fig. 27.

The first simulations of nuclear fragmentation based on percolation theory are due to Campi and Desbois (1984,1985), Bauer et al. (1986) and Biro, Knoll and Richert (1986). In the following, we will discuss briefly only the first two works.

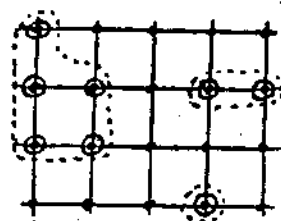


FIGURE 27

6.3 - Exotic Configurations in Percolation Approach

When the dices begin to decide whether the sites are

occupied or not, they don't care whether the clusters may assume or not quite exotic configurations. In consequence, we can find clusters like that (Fig. 28).

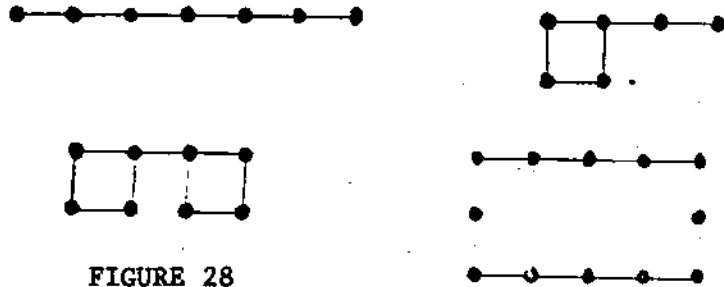


FIGURE 28

These clusters hardly can be identified with nuclear fragments, at least with the final state nuclei. At most, one may associate them with excited primordial fragments, but in this case one has necessarily to let them to evaporate.

One possible way to deal with such exotic clusters has been proposed by Campi and Desbois (1984,1985). Considering the nucleon Fermi motion, they have imposed "compactness" conditions on every cluster with A nucleons, both in configuration and momentum space, i.e.,

$$\left[\frac{1}{A} \sum_{i=1}^A (\vec{r}_i - \frac{1}{A} \sum_{j=1}^A \vec{r}_j)^2 \right]^{1/2} \leq (1+\epsilon) r_0 A^{1/3} \quad (48)$$

$$\left[\frac{1}{A} \sum_{i=1}^A (\vec{k}_i - \frac{1}{A} \sum_{j=1}^A \vec{k}_j)^2 \right]^{1/2} \leq (1+\epsilon) \sqrt{\frac{3}{5}} k_F \quad (48)$$

where k_F is the Fermi momentum, $r_0 = 1.2$ fm and $\epsilon \approx 0.1$. Adopting site percolation in a simple cubic lattice, they have found a percolation threshold $p_c \approx 0.60$. The fragment multiplicities $n(A,p)$ are given in Fig.29 as function of A , for different values of the concentration p . We can see that for small p , only

light fragments are formed and with increasing p heavier fragments are builded up, so that for large p , only light and heavy clusters are observed. This is just what has to be expected.

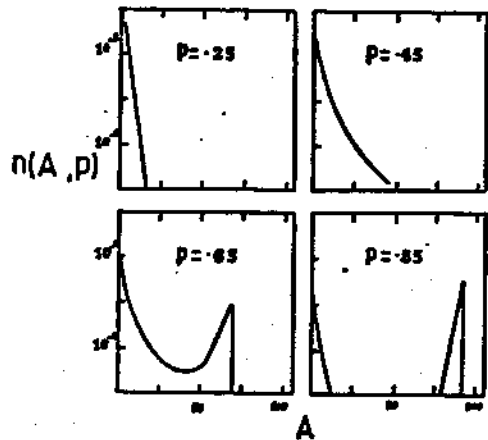


FIGURE 29 - Taken from Campi and Desbois (1984).

In Fig. 30, the mass yield σ is shown as function of $x = A/A_T$, where A_T is the target mass number. The result of their calculation (histogram) are compared with the experimental data (dot line) of $p+^{109}\text{Ag}$ reaction (English G. et al., 1974).

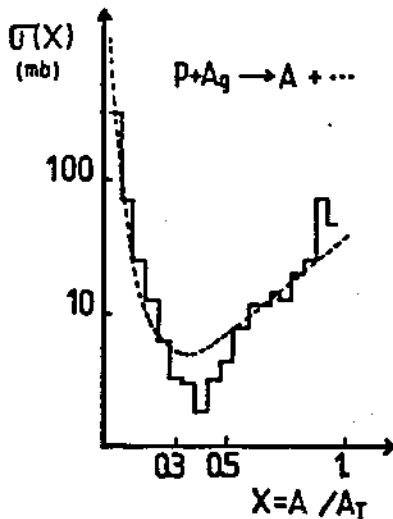


FIGURE 30 - Taken from Campi and Desbois (1984).

On the other hand, in order to exploit as much as possible the geometry, a very simple topological way has been proposed by Chao and Chung (1988), namely, the so-called tetrahedron percolation model. In what follows, we will summarize the main ingredients of this approach.

Let's consider a finite sphere containing A_0 sites arranged on an fcc lattice of size d . A certain fraction of sites $A = p A_0$ is occupied by nucleons.

The nucleons in a cluster are constrained to a tetrahedron linkage. A partition of the system is obtained by, first, looking for all possible groups of four nucleons in a tetrahedron binding and, second, combining two different clusters into a single one, when they have at least one nucleon in common (model I)

or at least two nucleons in common (Model II). The Model II is more suited than the Model I for allowing compact fragments to be formed.

Evaporation and other secondary effects are expected, at least in part, to be taken into account through the geometry, since the tetrahedron linkage constraint forbids the build-up of very dilute and ramified clusters.

The authors have performed calculations for a system with $A_0 = 87$ nucleons, and found that the mass distribution curves for small-to-medium fragments follow a power-law. This is illustrated in Fig. 31 for $p = 0.724$ (dots) and $p = 0.805$ (crosses) in the case of Model II. Fig. 32 shows the curves of

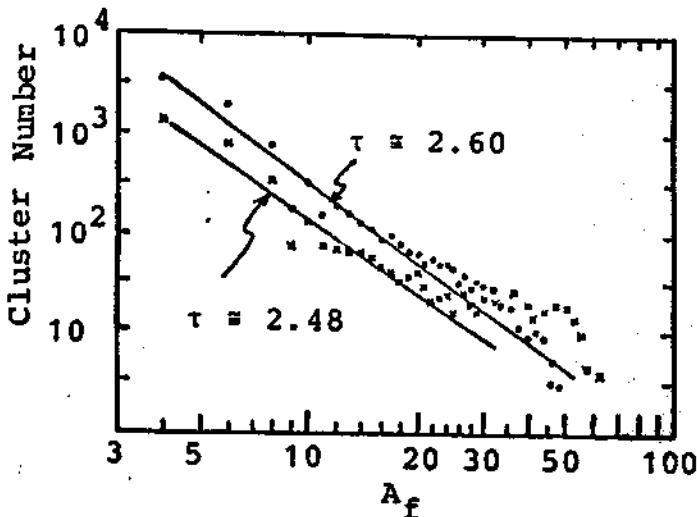


FIGURE 31 - Taken from Chao and Chung (1988 a).

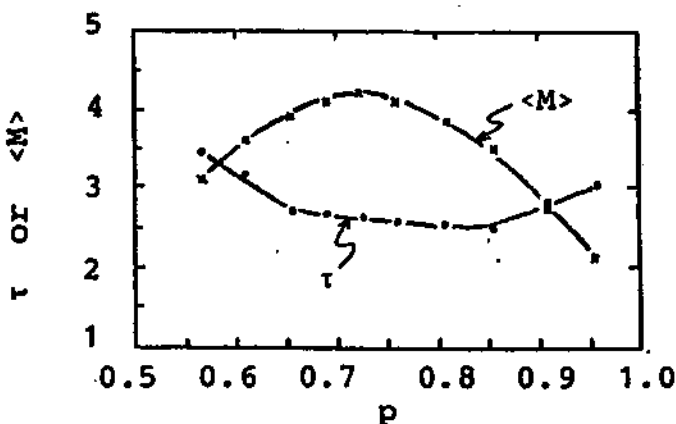


FIGURE 32 - Taken from Chao and Chung (1988 a).

τ and $\langle M \rangle$ as function of p also in the case of Model II. It is observed that for $0.66 < p < 0.79$, the values of τ are practically constant (2.6 - 2.7) and $\langle M \rangle \approx 4$ in this range. In Fig. 33, the same quantities are plotted for the case of $A_0 = 135, 201$ and volume expansion. In this last case, they consider that the nucleus thermalizes with a volume expansion be-

fore undergoing fragmentation. The calculations are performed with 135 nucleons occupying spherical volume containing 141, 177, 201, 225 and 249 sites, with corresponding values of $p = 0.957, 0.763, 0.672, 0.600$ and 0.542 .

The energy spectra of ^{12}C fragments for $p+\text{Kr}$ collisions are also computed within the tetrahedron percolation model, in which the dependence of the concentration p on the impact parameter was taken into account (Fig. 34).

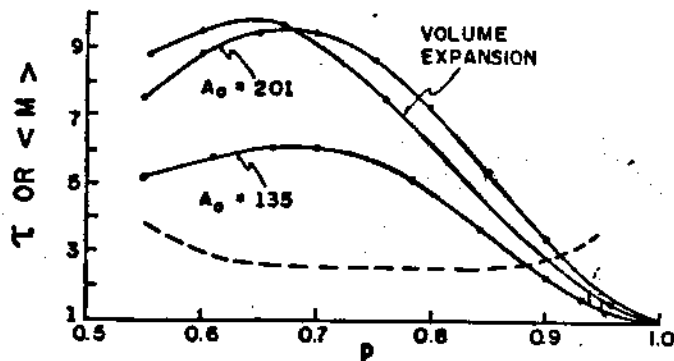


FIGURE 33 - Taken from Chao and Chung(1988 b).

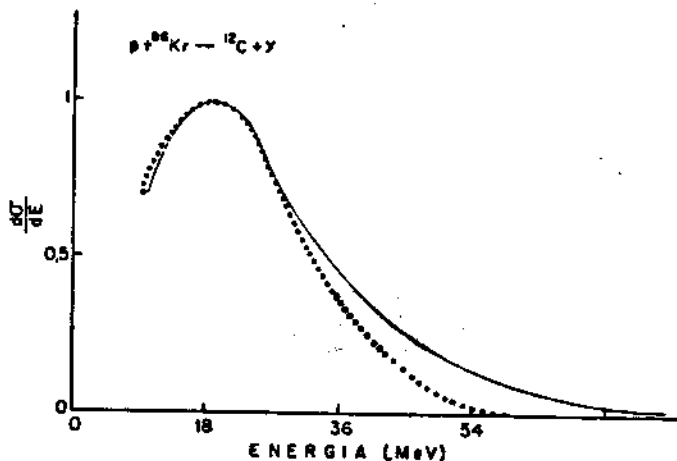


FIGURE 34 - Taken from Faulhaber (1989).

6.4. PERCOLATION WITH SECONDARY EVAPORATION

If the philosophy is to extend as much as possible

the geometrical approach, the exotic configurations may be dealt also by coupling an usual evaporation treatment to each cluster obtained by conventional percolation methods. In this regard, Santiago and Chung (1989) have made calculations with a conventional site percolation procedure. The evaporation from excited fragments is treated by the Weisskopf's statistical theory (Weisskopf, 1937). For simplicity, they have assumed that the evaporation timescale is much larger than the dynamical expansion timescale, so that the evaporation processes can be switch on solely after the whole expansion stage is completed.

The mass yield is shown in Fig. 35, where the open circles denote primordial yields (before evaporation) and the bold circle, the final yields (after evaporation). Also, it is shown in Fig. 36 ^{12}C kinetic energy spectra (dot line), compared with the experimental data of Hirsch et al., 1984 (solid line). The agreement seems very fine, even in the high energy region of the spectrum. However, the temperature ($\sim 11\text{MeV}$)

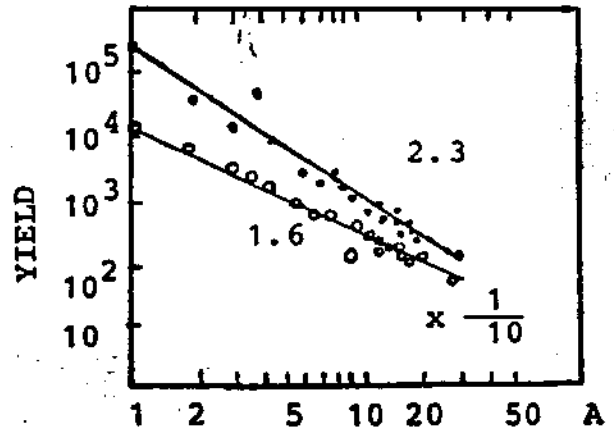


FIGURE 35 - From Santiago and Chung (1989).

necessary to fit the data is much higher than the maximum value found experimentally in excited nuclei, although lower than the value used by Friedmann and Lynch.

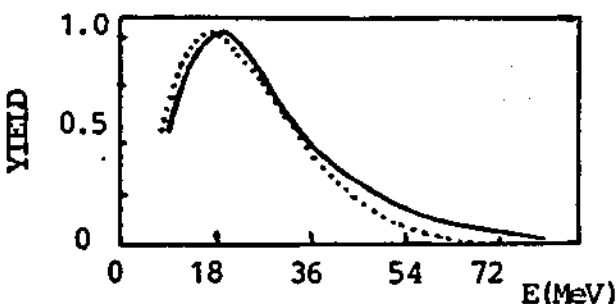


FIGURE 36 - Taken from Santiago and Chung (1989).

6.5. EVENT-BY-EVENT ANALYSIS

In the case of N events, eq. (46) for the moment of the mass distribution actually is written as

$$M_m(p) = \sum_s s^k \left[\frac{1}{N} \sum_{i=1}^N n_i(s,p) \right] \quad (50)$$

where the quantity in brackets is an average over many events for fixed p and $n_i(s,p)$ is the number of s -clusters in the single event i .

However, as p is not an experimental observable, we have no way to classify the events according to p , so that it is difficult to use directly Eq. (50) for analysing experimental data. In order to avoid this difficulty, Campi (1986) has proposed the so-called event-by-event analysis, in which Eq. (46) is applied for each event separately, i.e.,

$$M_k^i(p) = \sum_s s^k n_i(s,p) \quad (51)$$

In this manner, we can plot different moments versus each other, independent of the value of p . For example, Campi (1988), analysing the experimental data of Waddington and Freier (1985), has produced the Fig. 37, in which the second moment M_2 is plotted against the reduced multiplicity n . Using bond percolation, he computed M_2 for one-

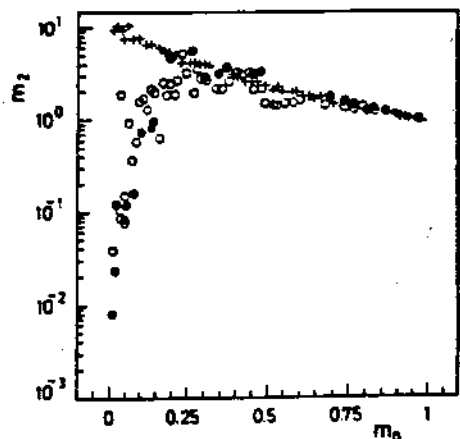


FIGURE 37 - Taken from Campi (1988).

-dimensional (crosses) and three-dimensional simple cubic lattice (open circles) cases. The full circles represent the value of M_2 obtained by using the above mentioned experimental data.

From the percolation theory, we know that in one dimension systems there is no phase transition (cf. Sect.6.1). This is just the opposite we find in the three dimension simple cubic lattice case, where a sharp second order phase transition is expected to occur. Fig.37 shows that M_2 is qualitatively the same for the experimental data and the three-dimensional system, but different from the one-dimensional case.

Furthermore, Campi claims that the existence of a maximum of M_2 is a manifestation of a phase transition, i.e, a percolative phase transition.

In the same direction, Bauer (1988) has proposed in the case of finite systems that Eq.(51) must be truncated, before the clusters in the sum reach the size of the system. As a matter of fact, he has found that the cut-off size should be $s_{cut} = A_T/2$. In order to investigate the question of the signature of a phase transition in finite systems, he also plotted (Fig.38) the $\ln M_2$ versus multiplicity (M_0), calculated with 5000 simulations and $s_{cut} = 30$, for a system of $A_0=108$. In Fig.38a, only undercritical events (i.e, corresponding to $p < p_c = 0.7$) and in Fig.38b, both undercritical as well as critical and overcriti-

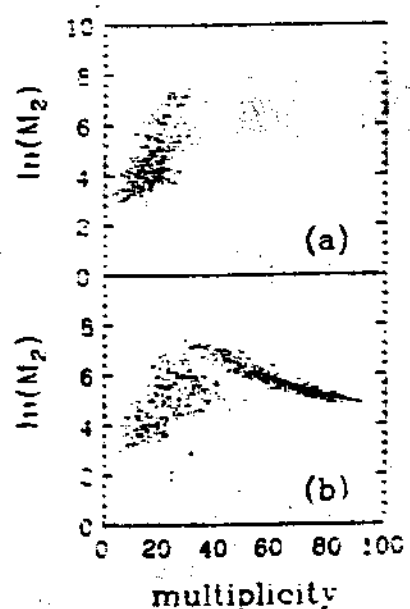


FIGURE 38 - Taken from Bauer (1988).

cal events were considered. He claims that the appearance of a maximum of M_2 has to be interpreted as a signature of a phase transition.

VII. SUMMARY AND CONCLUSIONS

The main experimental results of nuclear fragmentation are given as mass spectra, energy spectra and isotopic yield. In particular, it was shown that the mass spectra display a power-law. Several theoretical models were proposed and, in spite of the quite different assumptions, all of them seem to be able to reproduce with comparable error the existing data. This situation may be simply a consequence of the inclusive character of the experimental data.

It was suggested that the power-law behaviour of the mass yield is a manifestation of a liquid-gas phase transition, but this interpretation is still very controversial. On the other hand, as the same power law can be obtained in percolation models, it was proposed that moments of the mass distribution can display a signature of a percolative phase transition.

It is obvious that nuclei are not lattices, but it is certain that percolation ideas may be very useful in nuclear fragmentation. However, it remains to be accomplished the non easy task of relating the concentration p with the dynamic of the process, e.g., the fundamental nucleon-nucleon interactions, projectile energy or target excitation energy. One step toward this goal is given by Barz et al. (1986) who relate the probability p with the expanded volume of the nuclear system.

ACKNOWLEDGMENT

I would like to thank A.J.Santiago for his help in the preparation of this manuscript.

REFERENCES

1. Aichelin, J.; Hüfner, J. and Ibarra, R., Phys. Rev. C30, 107 (1984).
2. Aichelin, J.; Peilert, G.; Bohnet, A.; Rosenhauer, A.; Stöcker, H. and Greiner, W., Phys. Rev. C37, 2451 (1988).
3. Barz, H.W.; Bondorf, J.P.; Donangelo, R.; Mishustin, I.N. and Schulz, H., Nucl. Phys. A448, 753 (1986).
4. Barz, H.W.; Bondorf, J.P.; Donangelo, R.; Schulz, H., Phys. Lett. 169B, 318 (1986).
5. Bauer, W.; Post, U.; Dean, D.R. and Mosel, U., Nucl. Phys. A452, 699 (1986).
6. Bauer, W., Phys. Rev. C38, 1297 (1988).
7. Baym, G., Physica 96A, 131 (1979).
8. Berthier, B.; Boisgard, R.; Julien, J.; Hisleur, J.M; Lucas, R.; Mazur, C.; Ngõ, C.; and Ribrag, M., Phys. Lett. 193B, 417 (1987).
9. Bondorf, J.P.; Donangelo, R.; Mishustin, I.N.; Pethick, C. J.; Schulz, H. and Sneppen, K., Nucl. Phys. A443, 321 (1985a).
10. Bondorf, J.P.; Donangelo, R.; Mishustin, I.N.; Pethick, C. J. and Schulz, H., Nucl. Phys. A444, 460 (1985b).
11. Biro, T.S.; Knoll, J. and Richert, J., Nucl. Phys. A459, 692 (1986).
12. Boal, D.H., Phys. Rev. C30, 119 (1984).
13. Bock, I.; Lynen, U.; Pelta, D.; Winkler, U.; Glasow, R.; Kampert, K.H.; Santo, R.; Mueller, W.F.J.; Gobbi, A.; Hildenbrand, K.D.; Olmi, A.; Sann, H. and Stelzer, H., GSI Report, p.28 (1982).
14. Campi, X. and Desbois, J., Proceedings of the 7th High

- Energy Heavy Ion Study, GSI, Darmstadt (1984).
15. Campi, X. and Desbois, J., Proceedings of the 23 International Winter Meeting on Nuclear Physics, Bormio (1985).
 16. Campi, X., J. Phys.A 19, 917 (1986).
 17. Campi, X., Phys. Lett. B208, 351 (1988).
 18. Chao, N.C. and Chung, K.C., Proceedings of the Third International Conference on Nucleus-Nucleus Collisions, Saint-Malo, France (1988a).
 19. Chao, N.C. and Chung, K.C., Proceedings of the V International Conference on Clustering Aspects in Nuclear and Subnuclear Systems, Kyoto, Japan (1988b).
 20. Chung, K.C.; Donangelo, R. and Schechter, H., Phys. Rev. C36, 986 (1987).
 21. English, G.; Porile, N.T. and Steinberg, E.P., Phys. Rev. C10, 2268 (1974).
 22. Essam, J.W., Rep. Prog. Phys. 43, 883 (1980).
 23. Faulhaber, J.C.R., Ms.Sc. dissertation, CBPF (1989).
 24. Finn, J.E.; Agarwal, S.; Bujak, A.; Chuang, J.; Gutay, L.J.; Hirsch, A.S.; Minich, R.W.; Porile, N.T.; Scharenberg, R.P.; Stringfellow, B.C. and Turkot, F., Phys. Rev. Lett. 49, 1321 (1982).
 25. Fisher, M.E., Physics 3, 265 (1967).
 26. Friedmann, W.A. and Lynch, W.G., Phys. Rev. C28, 16 (1983a).
 27. Friedmann, W.A. and Lynch, W.G., Phys. Rev. C28, 950 (1983b).
 28. Glendenning, N.K.; Csernai, L.P. and Kapusta, J.I., Phys. Rev. C33, 1299 (1986).
 29. Gutbrod, H.H.; Warwick, A.I. and Wieman, H., Nucl. Phys. A387, 177c (1982).
 30. Hirsch, A.S.; Bujak, A.; Finn, J.E.; Gutay, L.J.; Minich, R.W.; Porile, N.T.; Scharenberg, R.P. and Stringfellow, B.C., Phys. Rev. C29, 508 (1984).
 31. Hirsch, A.S.; Bujak, A.; Finn, J.E.; Gutay, L.J.; Minich, R.W.; Porile, N.T.; Scharenberg, R.P.; Stringfellow, B.C., Nucl. Phys. A418, 267 (1984).
 32. Hüfner, J. and Mukhopadhyay, D., Phys. Lett. B173, 373 (1986).
 33. Jaqaman, R.H.; Mekjian, A.Z. and Zamick, L., Phys. Rev. C27, 2782 (1983).

34. Kirkpatrick, S., *Rev. Mod. Phys.* 45, 574 (1973).
35. Landau, L.D. and Lifshitz, E.M., *Statistical Physics, Vol. 5*, Addison-Wesley, Chap.VIII (1964).
36. Leray, S.J., *J. Phys.* C4, 275 (1986).
37. Mahi, M.; Bujak, A.T.; Carmony, D.D.; Chung, Y.H.; Gutay, L.J.; Hirsch, A.S.; Paderewski, G.L.; Porile, N.T.; Sangster, T.C.; Scharenberg, R.P. and Stringfellow, B.C., *Phys. Rev. Lett.* 19, 1936 (1988).
38. Minich, R.W.; Agarwal, S.; Bujak, A.; Chuang, J.; Finn, J. E.; Gutay, L.J.; Hirsch, A.S.; Porile, N.T.; Sharenberg, R.P. and Stringfellow, B.C., *Phys. Lett.* 118B, 458 (1982).
39. Ngõ, C.; Boisgard, R.; Desbois, J.; Nemeth, J.; Barranco, M. and Mathiot, J.F., *Nucl. Phys.* A471, 381c (1987).
40. Ngõ, C.; Cerruti, C.; Desbois, J.; Boisgard, R.; Natowitz, J. and Nemeth, J., *Nucl. Phys.* A476, 74 (1988).
41. Panagiotou, A.D.; Curtin, M.W. and Scott, D.K., *Phys. Rev.* C31, 55 (1985).
42. Ravenhall, D.G.; Pethick, C.J. and Lattimer, J. M., *Nucl. Phys.* A407, 572 (1983).
43. Santiago, A.J. and Chung, K.C., *Proceedings of the International Nuclear Physics Conference, São Paulo* (1989).
44. Schlagel, T.J. and Pandharipande, V.R., *Phys. Rev.* C36, 162 (1987).
45. Stauffer, D., *Introduction to Percolation Theory*, Taylor and Francis (1985).
46. Vicentini, A.; Jacucci, G. and Pandharipande, V.R., *Phys. Rev.* C31, 1783 (1985).
47. Waddington, C.J. and Freier, P.S., *Phys. Rev.* C31, 888 (1985).
48. Warwick, A.I.; Wieman, H.H.; Gutbrod, H.H.; Maier, M.R.; Peter, J.; Ritter, H.G.; Stelzer, H. and Weik, F., *Phys. Lett.* 48, 1719 (1982).
49. Warwick, A.I.; Wieman, H.H.; Gutbrod, H.H.; Maier, M.R., Peter, J.; Ritter, H.G.; Stelzer, H. and Weik, F., *Phys. Rev.* C27, 1085 (1983).
50. Weisskopf, V., *Phys. Rev.* 52, 295 (1937).